CrossMark

RESEARCH

Elastic and thermodynamical properties of cubic (3*C*) silicon carbide under high pressure and high temperature

Dinesh Varshney[1] · S. Shriya[1] · M. Varshney[2] · N. Singh[3] · R. Khenata[4]

Abstract Pressure-dependent first-order phase transition, mechanical, elastic, and thermodynamical properties of cubic zinc blende to rock-salt structures in 3*C* silicon carbide (SiC) are presented. An effective interatomic interaction potential for SiC is formulated. The potential for SiC incorporates long-range Coulomb, charge transfer interactions, covalency effect, Hafemeister and Flygare type short-range overlap repulsion extended up to the second-neighbour ions, van der Waals interactions and zero point energy effects. The developed potential including many body non-central forces validates the Cauchy discrepancy successfully to explain the high-pressure structural transition, and associated volume collapse. The 3*C* SiC ceramics lattice infers mechanical stiffening, thermal softening, and ductile (brittle) nature from the pressure (temperature) dependent elastic constants behaviour. To our knowledge, these are the first quantitative theoretical predictions of the pressure and temperature dependence of mechanical and thermodynamical properties explicitly the mechanical stiffening, thermally softening, and brittle/ductile nature of 3*C* SiC and still awaits experimental confirmations.

Introduction

Silicon carbide, (SiC), a high quality technical grade ceramics, possesses wide energy band gap, low density, high strength, low thermal expansion, high thermal conductivity, high hardness, high melting point, large bulk modulus, low dielectric constant, high elastic modulus, excellent thermal shock resistance, and superior chemical inertness. The IV–IV SiC compound possesses tetrahedral of C and Si atoms with strong bonds in the crystal lattice and the availability of wide variety of its polytypes with unique structural and electronic properties. SiC has been a subject of immense interest as it is a very hard and strong ceramics with its application in requiring high endurance, such as car brakes and clutches and ceramics plates in bulletproof vests. The high thermal conductivity coupled with low thermal expansion and high strength gives this material exceptional thermal shock resistant qualities. Ceramics SiC with little or no grain boundary impurities maintain strength at very high temperatures with no strength loss [1, 2].

The structural transition, mechanical and elastic properties under low and high pressures of SiC have attracted much interest in both experimental [3, 4] and theoretical [5–15] investigations to elucidate the pressure-dependent behaviour of polytype [cubic (3*C*), hexagonal (6*H*), and rhombohedral (15*R*)] SiC. The energy-dispersive X-ray

✉ Dinesh Varshney
vdinesh33@rediffmail.com

[1] Materials Science Laboratory, School of Physics, Vigyan Bhavan, Devi Ahilya University, Khandwa Road Campus, Indore 452001, India

[2] Department of Physics, M. B. Khalsa College, Indore 452002, India

[3] Department of Physics, Ranchi College, Ranchi, Jharkhand 834008, India

[4] Laboratoire de Physique Quantique et de Modélisation Mathématique (LPQ3M), Département de Technologie, Université de Mascara, 29000 Mascara, Algeria

diffraction with a diamond anvil cell has identified structural transformation in $3C$ SiC [zinc-blende (ZB) ($B3$) structure to the rock-salt ($B1$) structure $\approx$ 100 GPa] with a volume collapse of about 20.3 % [3]. The transition is reversible and the zinc-blende phase is recovered below 35 GPa upon decompression. Furthermore, $6H$ polytype SiC is found to be stable up to about 90.0 GPa. Later, shock compression experiments on $6H$ SiC show a first-order phase transition into a sixfold coordinated rock-salt structure around 105 ± 4 GPa with a volume reduction of about 15 ± 3 % [4].

Structural and thermal stability as well as high-pressure behaviour of $3C$-SiC has been described both by ab initio [5–7, 11, 14, 16] and molecular dynamics simulations [8, 10, 15]. Based on ab initio density functional calculations with the local-density approximation (LDA) show that the transition pressure of $3C$-SiC is around 60 GPa [ZB to rock salt (RS)] [5–7, 11–14, 16]. Following Perdew–Wang generalized gradient approximation (GGA) for the exchange-correlation potential and the Troullier–Martins pseudopotentials; the transition pressure of SiC at about 63 GPa is predicted [6, 12, 13]. Using the Troullier–Martins pseudopotentials and the LDA, the phase-transition pressure of 100 GPa is also documented [7, 14]. It is noted that first-principles LDA calculations underestimate critical pressure for structural phase transition.

The constant-pressure molecular dynamics (MD) simulation retraces the reversible phase transformation [$3C$ to RS] in SiC [8]. The first-principle calculations clearly demonstrate the structural transformation of SiC from a fourfold coordinated structure to sixfold coordinated structure under pressure. The phase transition from the zinc-blende phase to the RS phase is associated with a cubic to only one intermediate state as monoclinic unit cell transformation. Later on, the structural phase transition and mechanical properties of SiC from the ZB structure to the RS structure under pressure are investigated in detail by the first-principles plane-wave pseudopotential density functional theory method [9]. The results on the high-pressure elastic constants illustrate that the ZB structure SiC is found unstable when the applied pressure is larger than 126.6 GPa consistent with the experimental data and the molecular dynamics (MD) simulation results.

The molecular dynamics with effective interatomic interaction potential for SiC incorporating two-body and three-body covalent interactions is also proposed. The covalent characteristics SiC are described by the three-body potential using modified Stillinger–Weber form. The molecular dynamics method with the developed interaction potential is employed to investigate the structural and dynamical properties of crystalline $3C$, amorphous, and liquid states of SiC for several densities and temperatures [10, 15]. The phase stability of SiC under high pressure and behaviour of elastic constants with temperature is worth for microscopic understanding as well as technological applications.

The quantum computations based on density functional theory (DFT) as the full-relativistic version of the full-potential augmented plane-wave plus local orbitals method (FP − APW + lo) are powerful techniques and have the advantage of elucidating the ground state properties not only for small atomic systems but also for large molecules [17]. Density functional theory with approximate local and semilocal density functionals with nonlocal and long-range Coulomb interactions are effective for dense molecules and materials as well as short-range interactions for soft matter, van der Waals complexes, and biomolecules [18].

The quantum mechanical calculations suggest a favourable phase transition into a RS structure with different transition pressure for $3C$ SiC. However, these underestimate critical pressure for structural phase transition. We thus aimed at computing the pressure-induced phase transition of $3C$ SiC by formulating an effective interatomic potential. Note that the determination of ground state properties of IV–IV compounds with complex bonds based on lattice dynamical models is not easy. One needs to take care of experimental data with high accuracy and precision that accounts for low degree of freedom. The object of the proposed investigation is to develop a differential model as well to integrate the observed effect enabling useful prediction with reduced input experimental parameters.

The lattice dynamical models are useful in yielding both qualitative and quantitative information also with suggestive parameterization of the materials parameter. The density functional quantum calculations need precisely structural information as atomic positions and space groups. It also cares the value of volume around the experimental volume of the system. The successive iteration is thus made to determine the total energy corresponding to this volume. The thermal equation of state is needed to determine the ground state structural properties. It includes the lattice parameters within stable structure, the bulk modulus and pressure derivatives of elastic constants. The transition pressure is obtained by the common tangent between the two pressure–volume curves.

While exploring the ground state and anharmonic properties of simple and complex molecules, two major methods, one based on analytical form of cohesion with effective physical understanding and other based on expensive and time taking computational methods, are progressive. In the analytical models with two body interactions, the force constant deduced does not validate the Cauchy discrepancy. Incorporating many body interactions in the interaction potential with different cohesive energy forms is seen as the relevant potential which validates the Cauchy discrepancy. It is thus the major objective to seek the importance of both

charge transfer interactions and covalent nature apart from zero point energy effects of group IV–IV cubic SiC in the interaction potential.

While discussing the mechanical and thermodynamical properties, the lattice dynamical model based on charge transfer interactions has been found successful [19–26]. The overlap repulsion potential (extended up to second-neighbour ions) is based on Hafemeister and Flygare [27]. The short-range interactions as the induced charge dipole–dipole and charge dipole–quadruple (van der Waals) interaction are found to be successful to determine the cohesion in several alkaline-earth solids [28]. As far as the pressure (temperature) induced mechanical and elastic properties as hardness, ductile nature, mechanical stiffening and thermal softening of SiC ceramics is concerned, these are probably the first quantitative theoretical prediction of its kind and still awaits experimental confirmations. Deduced aggregate Young's modulus, compression and shear wave velocities are in agreement with the observed values.

The opportunities offered by SiC ceramics have, therefore, motivated large research efforts which in turn have addressed only structural transitions and elastic, thermal and thermodynamical properties are still lagging. The proposed studies are organized in the following sequence. We first discuss the key assumptions to develop an effective interatomic potential between a pair of ions. We then support them by physical arguments for ceramics SiC followed by an equation of state in "Computational methodology" section. The Slater–Kirkwood variational method is employed to determine the induced charge dipole–dipole and charge dipole–quadruple (van der Waals) coefficients keeping in mind that both ions (Si and C) are polarizable. In sequence, we compute phase-transition pressures, the second-order aggregate elastic constants within the Shell model. Thus, the importance of long-range Coulomb with charge transfer interactions, covalent nature of bonds, charge dipole–dipole and charge dipole–quadruple (van der Waals) interaction, and the short-range overlap repulsive interaction up to second-neighbour ions is validated. In "Results and discussion" section, we discuss the various elastic properties.

As regard the ceramics 3C SiC, a number of works have been made on the structural stability of high-pressure phases but the pressure and temperature-dependent properties are sparse as normalized volume, aggregate second-order elastic constants C_{ij}, Bulk modulus B_T, Cauchy discrepancy in second-order elastic constant Δ_1^2, second-order elastic constant anisotropy γ_1^2, melting temperature T_M, aggregate third-order elastic constants C_{ijk}, Cauchy discrepancy Δ_i^3 in third-order elastic constant, third-order elastic anisotropy γ_i^3, isotropic shear modulus G_H, Voigt's shear modulus G_V, Reuss's shear modulus G_R, Young's modulus E, Poisson's ratio ν and Pugh ratio ϕ (=B_T/G_H)

leading to ductility (brittleness), Lamé's constant λ and μ, and elastic wave velocity v_l and v_s.

The anharmonic effects on SiC lattice are further studied by investigating the Gruneisen parameter γ_G, isothermal compressibility β, Debye temperature θ_D, hardness H_V, heat capacity C_v, and thermal expansion coefficient $\alpha_{th.exp.}$ either in ZB or RS structures. The relevant expressions are documented in Appendix 1 and 2. We also provide a comparison of computed values with observed experimental and other theoretical studies. The major conclusions are presented in "Concluding remarks" section.

Computational methodology

To study the phase stability and the aggregate elastic constants of SiC under high pressures, we formulate an interatomic potential. The proposed interaction potential is based on the following assumptions: variations in force constants of Si and C are small, the short-range interactions between Si and C atoms are effective up to their second-neighbour ions, and harmonic elastic forces are viable for a pair of atoms without any internal strains within the crystal. Application of mechanical pressure as external variable causes an increase in the overlap of adjacent ions in a crystal. The result is a charge transfer takes place between the overlapping electron shells of Si and C atoms. The transferred charges interact with neighbouring charges around the lattice via Coulomb's law. Also, the chemical bonds in SiC are both ionic and covalent in nature and the application of pressure causes change in crystal structure (first-order structural phase transition), volume collapse and elastic properties.

The proposed interatomic potential is thus a route to discuss the structural transitions, mechanical properties in particularly, about stiffness, softness, ductile, brittle nature, elastic constants anisotropy, compression and shear elastic wave velocity. In addition, the potential is predictive to explain the validity of non-central forces and anharmonicity from thermodynamical properties namely Debye temperature, heat capacity and thermal expansion coefficient of 3C SiC. At zero pressure and variable temperature, the underlined effective interatomic potential also describes some of the temperature-induced thermal and thermodynamical properties of 3C SiC.

The effective interatomic potential at ambient pressure invokes an isolated stable phase when the crystal free energy is minimized for the specified thermodynamic conditions. For this purpose, if the variables such as temperature, pressure or magnetic field applied on the crystal are altered, either the free energy changes smoothly and continuously or discontinuously. Variations in free energy cause structural phase transition. The SiC ceramics transform from their initial $B3$ to $B1$ structure under pressure.

The minimum Gibbs's free energy, G, infers the stability of a particular structure. Herein, Gibbs's free energy, $G = U + PV - TS$. The notations are: U is internal energy, which at 0 K is the cohesive energy, S is the vibrational entropy at absolute temperature T, pressure P and volume V. The thermodynamically stable phase at a given pressure P and at zero temperature is the one with lowest enthalpy. The thermodynamical potential is thus the Helmholtz free energy (H).

The interatomic potential with pressure or temperature as thermodynamical variable requires the estimation of the Gibbs's free energies for ZnS ($B3$) phase and NaCl ($B1$) phase. We use Born equation: $G_{B3}(r) = U_{B3}(r) + 3.08Pr^3$ for ZnS ($B3$) phase and $G_{B1}(r') = U_{B1}(r') + 2Pr'^3$ for NaCl ($B1$) phase. At phase-transition pressure P and at zero temperature: $G_{B1} = G_{B3}$ [29]. The notations $U_{B3}(r)$ infer the total potential energy of ZnS ($B3$) phase and $U_{B1}(r')$ as total potential energy for the RS ($B1$) phase. The unit cell volumes are V_{B3} ($=3.08r^3$) and V_{B1} ($=2\,r'^3$). The nearest neighbour distance is r (r') in ZB (RS) structure. The total potential energy for ZnS ($B3$) and NaCl ($B1$) phases is

$$
\begin{aligned}
U_{B3} = {} & (-\alpha_M Ze^2/r)[Z + 2nf(r)] - Cr^{-6} - Dr^{-8} \\
& + nb\beta_{ij}\exp\big[(r_i + r_j - r_{ij})/\rho\big] \\
& + (n'b/2)\big[\beta_{ii}\exp\big((2r_i - kr_{ij})/\rho\big) \\
& + \beta_{jj}\exp\big((2r_j - kr_{ij})/\rho\big)\big] + \big[\{\hbar < \omega^2 >^{1/2}/2\}\big]
\end{aligned} \quad (1)
$$

$$
\begin{aligned}
U_{B1} = {} & (-\alpha'_M Ze^2/r')[Z + 2mf(r')] - Cr'^{-6} - Dr'^{-8} \\
& + mb\beta_{ij}\exp\big[(r_i + r_j - r'_{ij})/\rho\big] \\
& + (m'b/2)\big[\beta_{ii}\exp\big((2r_i - k'r'_{ii})/\rho\big) \\
& + \beta_{jj}\exp\big((2r_j - k'r'_{jj})/\rho\big)\big] + \big[\{\hbar < \omega^2 >^{1/2}/2\}\big]
\end{aligned} \quad (2)
$$

Due to complex nature of bonds in SiC, the ionic charge for Si and C atom cannot be determined uniquely. The calculation of the Madelung energy is thus modified by incorporating the covalency effects [10, 15, 30, 31]. The charge in above equations is thus written incorporating the polarization of a spherical shaped dielectric in displacing the constituent positive ions. The charge transfer interactions caused by the deformation of the electron shells of the overlapping ions and the covalency effects are the major attributes of long-range Coulomb effects. The IV–IV semiconducting compound contains covalent bonds so that some electrons are distributed over the region between neighbouring atoms; in such situation the interaction energies are attributed from the contribution of charge dipole-dipole and charge dipole-quadrupole terms. The induced charge dipole–dipole and charge dipole–quadruple (van der Waals) interactions are the third and fourth terms which are the short-range vdW attractive potential energies.

The fifth and sixth terms are the short-range overlap repulsive energies. This is due to the overlap repulsion between ij, ii and jj ions. The Madelung constants for $B3$ ($B1$) phases are represented by α_m (α_m'). β_{ij} symbolized for Pauling coefficient and is defined as $\beta_{ij} = 1 + (Z_i/n_i) + (Z_j/n_j)$ with $Z_i(Z_j)$ and $n_i(n_j)$ as the valence and the number of electrons in the outermost orbit. The numbers of the nearest unlike n (=4) and like n' (=6) neighbours are for $B3$ (ZnS). Similarly, numbers of the nearest unlike m (=6) and like m' (=6) are for $B1$ (NaCl) structure. The Ze is being the ionic charge, k (k') is the structure factor for $B3$ ($B1$) structures, and b (ρ) is the hardness (range) parameters. We denote the nearest neighbour ion separations as r (r') for $B3$ ($B1$) structures.

The last term in Eqs. 1 and 2 is the lowest possible energy of the system and is due to the zero point energy. Here, $<\omega^2>^{1/2}$ ($=k_B\theta_D/\hbar$) is the mean square frequency related to the Debye temperature θ_D. The Debye temperature can be known either from Heat capacity measurements or from the Bulk modulus value using $\theta_D = (\hbar/k_B)\sqrt{(5r_0B_T/\mu)}$. Herein, r_0, B and μ are the equilibrium distance, Bulk modulus and reduced mass of the compounds. Henceforth, model potential for ground state incorporates the attractive, repulsive and zero point energy.

We use the variational approach to deduce the overall vdW coefficients C (charge dipole–dipole) and D (charge dipole–quadruple) [32]. The short-range vdW coefficients due to induced charge dipole–dipole and charge dipole–quadruple interactions caused by Si atom and C atom are

$$
c_{ij} = \frac{3}{2}\frac{e\hbar}{\sqrt{m_e}}\alpha_i\alpha_j\left[\left(\frac{\alpha_i}{N_i}\right)^{1/2} + \left(\frac{\alpha_j}{N_j}\right)^{1/2}\right]^{-1}, \quad (3)
$$

$$
d_{ij} = \frac{27}{8}\frac{\hbar^2}{m_e}\alpha_i\alpha_j\left[\left(\frac{\alpha_i}{N_i}\right)^{1/2} + \left(\frac{\alpha_j}{N_j}\right)^{1/2}\right]^2\left[\left(\frac{\alpha_i}{N_i}\right) + \frac{20}{3}\left(\frac{\alpha_i\alpha_j}{N_iN_j}\right)^{1/2} + \left(\frac{\alpha_j}{N_j}\right)\right]^{-1}. \quad (4)
$$

$$
c_{ii} = \frac{3}{2}\frac{e\hbar}{\sqrt{m_e}}\alpha_i\alpha_i\left[\left(\frac{\alpha_i}{N_i}\right)^{1/2} + \left(\frac{\alpha_i}{N_i}\right)^{1/2}\right]^{-1}, \quad (5)
$$

$$
d_{ii} = \frac{27}{8}\frac{\hbar^2}{m_e}\alpha_i\alpha_i\left[\left(\frac{\alpha_i}{N_i}\right)^{1/2} + \left(\frac{\alpha_i}{N_i}\right)^{1/2}\right]^2\left[\left(\frac{\alpha_i}{N_i}\right) + \frac{20}{3}\left(\frac{\alpha_i\alpha_i}{N_iN_i}\right)^{1/2} + \left(\frac{\alpha_i}{N_i}\right)\right]^{-1} \quad (6)
$$

$$
c_{jj} = \frac{3}{2}\frac{e\hbar}{\sqrt{m_e}}\alpha_j\alpha_j\left[\left(\frac{\alpha_j}{N_j}\right)^{1/2} + \left(\frac{\alpha_j}{N_j}\right)^{1/2}\right]^{-1}, \quad (7)
$$

$$
d_{jj} = \frac{27}{8}\frac{\hbar^2}{m_e}\alpha_j\alpha_j\left[\left(\frac{\alpha_j}{N_j}\right)^{1/2} + \left(\frac{\alpha_j}{N_j}\right)^{1/2}\right]^2\left[\left(\frac{\alpha_j}{N_j}\right) + \frac{20}{3}\left(\frac{\alpha_j\alpha_j}{N_jN_j}\right)^{1/2} + \left(\frac{\alpha_j}{N_j}\right)\right]^{-1}. \quad (8)
$$

In the above equations, the notations: m_e, e and Z are mass of the electron, charge and valence of the

constituent metallic element, respectively. The symbols α_i, and α_j represent the polarizabilities of ith and jth ion, respectively. The effective number of electrons responsible for polarization is symbolized by N_i and N_j. The lattice sums S_{ij} and T_{ij} enable one to compute the overall vdW coefficients C and D in terms of c and d values determined from Eqs. 1 to 8. The lattice sums S_{ij}, and T_{ij} are expressed as [28]:

$$C = c_{ij}S_{ij} + c_{ii}S_{ii} + c_{jj}S_{jj} \tag{9}$$

$$D = d_{ij}T_{ij} + d_{ii}T_{ii} + d_{jj}T_{jj} \tag{10}$$

SiC is a tetrahedrally coordinated covalent material and the complex chemical bonding corroborate both ionic and covalent nature. The Coulomb interaction between ions of Si and C atoms leads to charge transfer interactions. Apart from this, the covalent character of bond bending and stretching also needs to be incorporated in the potential. Thus, the second term in Eqs. 1 and 2 is an algebraic sum of non-central many body forces as the charge transfer force parameter and the force parameter arise due to covalent nature *i.e.* $f(r) = f_{cti} + f_{cov}$. The charge transfer between ions of Si and C atoms is denoted in terms of a force parameter f_{cti} and is expressed as [27, 33, 34]:

$$f_{cti} = f_0 \exp(-r/\rho) \tag{11}$$

Here, r_i (r_j) is the ionic radii of $i(j)$ ion.

The complex chemical bonding in IV–IV semiconducting compounds infers SiC as partially ionic and partially covalent in bonding. The attractive forces due to covalent nature thus modify the charge and are now the effective charge. The polarization effects originate from changes in covalency due to Si–Si, Si–C, and C–C interacting electric fields. The covalency term in the interaction potential is thus expressed as [30, 31]:

$$f_{\text{cov}}(r) = \frac{4e^2 V_{sp\sigma}^2}{r_0 E_g^3} \tag{12}$$

Here, $V_{sp\sigma}$ represents the transfer matrix element between the outermost p orbital and the lowest excited of s state. The transfer energy of electron from p to the s orbital is denoted as E_g. The effective charge e_S^* of SiC is related with the number of electrons transferred to the unoccupied orbitals from its surrounding nearest neighbour. The electron density is thus $n_c = 1 - e_S^*/e$. Thus, in SiC for overlap distortion effect $e_S^* \neq e$. The transfer matrix element $V_{sp\sigma}$ and the transfer energy E_g are related to electron density as $n_c/12 \cong V_{sp\sigma}^2/E_g^2$. The effective charge e_S^* is thus

$$\frac{V_{sp\sigma}^2}{E_g^2} = \frac{1 - e_s^*}{12} \tag{13}$$

The transfer energy E_g is

$$E_g = E - I + (2\alpha - 1)\frac{e^2}{r} \tag{14}$$

Here, E is the electron affinity for C and I is the ionisation potential of constituent atom.

The Szigeti effective charge e_S^* $(=Ze)^*$ is written in terms of the optical static dielectric constant ε_0 and the high frequency dielectric constant ε_∞ as [19–26]:

$$e_s^{*2} = \frac{9\mu\omega_{TO}^2(\varepsilon_0 - \varepsilon_\infty)}{4\pi N_k(\varepsilon_\infty + 2)^2} \tag{15}$$

and

$$\frac{e_s^{*2}}{e^2} = \frac{9V\mu\omega_{TO}^2(\varepsilon_0 - \varepsilon_\infty)}{4\pi e^2(\varepsilon_\infty + 2)^2} \tag{16}$$

The symbol μ is the reduced mass, N_k is the number of atoms present per unit cell volume i.e. $N_k = 1/V$, ω_{TO} is the long wavelength transverse optical phonon frequency. Thus, for 3C SiC e_S^* deviates from e and is attributed to covalent nature of Si–Si, Si–C, and C–C bonds.

Usually materials document a transition when the thermodynamic potential relevant to the given ensemble of the lower pressure phase equals that for some other structure in the absence of any barrier. The low pressure phase becomes the stable phase above this coexistence pressure. After determining the stable phase we also compute the higher order elastic constants, their pressure derivatives and anisotropy. The Appendix 1 illustrates the essential equations for the higher order elastic constants and their pressure derivatives. With these understanding of interatomic potential in SiC, we have four material parameters, namely, modified ionic charge, hardness, range, force parameter [Z_m, b, ρ, $f(r)$]. Values of them can be deduced from equilibrium conditions [35–42].

Results and discussion

The application of pressure, temperature and magnetic field probably transforms materials from one structure to another. The relative stability of two crystal structures requires an extremely accurate prediction. The interatomic interaction potential with charge transfer interactions caused by ions of Si and C atom and covalent nature of Si–Si, Si–C, and C–C bonds are effective in studying the structural phase transitions and elastic properties of tetrahedrally coordinated ceramics 3C SiC. We evaluate the phase transition pressure by computing the Gibbs free energy $G = U + PV - TS$ for the ZB and RS phases. We note that the Gibbs free energy is thus the enthalpy H ($=U + PV$) at $T = 0$ K.

While doing high-pressure experiments, the huge applied pressure causes a reduction of the material volume.

The temperature variations during the experiments will normally produce much smaller changes in the relative stabilities of different phases. Thus, the Gibbs free energy at zero temperature, which is the enthalpy H, is measured. The thermodynamically stable phase of crystal at 0 K and at ambient pressure P is the one with the lowest enthalpy. Thus, the zero-temperature theoretical calculations are valid with experiment. In a situation when temperature variations are large during experiment for certain materials the effects of finite temperature may be significant. With these assumptions, we investigate structural and elastic properties of SiC in an ordered way.

The thermodynamical potential G or H in SiC is computed involving modified ionic charge, hardness, range and charge transfer parameters [Z_m, b, ρ, $f(r)$] as [35–42]:

$$\left| \frac{dU(r)}{dr} \right|_{r=r_0} = 0 \qquad (17)$$

Also, the bulk modulus (B_T):

$$\left| \frac{d^2U(r)}{dr^2} \right|_{r=r_0} = (9kr_0)^{-1} B_T \qquad (18)$$

We first deduce vdW coefficients C and D involved in expressions (1) and (2) from the Slater–Kirkwood variational method [32], for 3C SiC ceramics material parameters, and are enlisted in Table 1. The charge dipole–dipole and charge dipole–quadruple vdW coefficients are influenced by electronic polarizabilities. The polarizability values have been obtained from least-squares fit of experimental refraction data using additive rule and a Lorentz factor of $4\pi/3$ [43, 44]. We consider that the SiC to be partially ionic and covalent to discuss their structural, mechanical, elastic and thermodynamical properties in a systematic manner.

As a next step, we use the experimental data on lattice constant (a) [45], the bulk modulus (B_T) [46], ionic (Ze), effective charge (e_s^*) and the second-order aggregate elastic constant C_{12} (C_{44}) [47] for determining the material parameters. Deduced values of hardness (b), range (ρ) parameter, and non-central many body forces arising due to charge transfer (f_{cti}) and covalency (f_{cov}) for 3C SiC ceramics are illustrated in Table 1. The effective charge e_S^* depends on the values of optical dielectric constant ε_s and the high frequency dielectric constant ε_∞. The value of long wave length transverse optical phonon frequency ω_{TO} is taken from [48] to have the effective charge e_S^* and hence the covalency contribution.

We then minimize the Gibbs's free energies $G_{B3}(r)$ and $G_{B1}(r')$ for the equilibrium interatomic spacing (r) and (r') to determine structural phase transition of SiC. Table 1 shows the optimized values of equilibrium interatomic spacing in $B1$ and $B1$ phases. The Gibbs's free energy $G_{B3}(r)$ [$G_{B1}(r')$] as functions of pressure (P) for SiC is

Table 1 Estimated and input crystal data: vdW coefficients [c_{ii}, c_{ij}, c_{jj}, C, d_{ii}, d_{ij}, d_{jj}, D], lattice constant (a_0), bulk modulus (B_T), second-order elastic constant C_{12} (C_{44}), optimized value of ionic radii r_i (r_j), hardness (b), range (ρ), charge transfer parameter $f(r)$, equilibrium distance: r_0 ($B3$); r_0' ($B1$), Gibbs's free energy: $G_{B3}(r)$; $G_{B1}(r)$

Input parameters	SiC
c_{ii} (10^{-60} erg cm^6)	28.76
c_{ij} (10^{-60} erg cm^6)	0.71
c_{jj} (10^{-60} erg cm^6)	0.047
C (10^{-60} erg cm^6)	14.07
d_{ii} (10^{-76} erg cm^8)	14.284
d_{ij} (10^{-76} erg cm^8)	0.297
d_{jj} (10^{-76} erg cm^8)	0.002718
D (10^{-76} erg cm^8)	3.019
a_0 (Å)	4.36 [45]
B_T (GPa)	227.0 [46]
C_{12} (GPa)	142.0 [47]
C_{44} (GPa)	256.0 [47]
r_i (Å)	0.42
r_j (Å)	1.162
b (10^{-12} erg)	7.512
ρ (10^{-9} cm)	3.29
$f(r)$ (10^{-3})	5.267
Equilibrium distance (Å) r_0 ($B3$)	1.89
Equilibrium distance (Å) r_0' ($B1$)	2.11
Gibb's free energy (kJ mol^{-1}) $G_{B3}(r)$	−4570
Gibb's free energy (kJ mol^{-1}) $G_{B1}(r)$	−4498

discerned in Fig. 1a. At zero pressure, the Gibb's free energy for SiC in $B3$ crystal phase is more negative. Thus, at zero pressure SiC in $B3$ phase is thermodynamically and mechanically stable, while the $B1$ is not. On the other hand, above the phase transition pressure ($P_T = 90$ GPa), the Gibb's free energy for $B1$ system becomes more negative than $B3$ phase, implying $B1$ phase will be more stable. The cohesive energy per particle is obtained as 6.301 eV for 3C SiC which is consistent with earlier experimental value of 6.34 eV [49]; 7.415 eV from ab initio density functional calculations and molecular dynamics method yields 6.3410868 eV for SiC [50].

The phase stability of cubic 3C SiC under high pressures is essentially based on material parameters namely hardness (b), range (ρ), non-central many body forces as charge transfer force (f_{cti}) and covalency parameter (f_{cov}). These are obtained from the experimental data. We comment that the available data based on one kind of experiment depend on the conditions of measurement. Henceforth, while developing a theory, one faces certain complications and one need to find suitable data that varies from technique to technique. For SiC, we pay special attention while

Fig. 1 Variation of Gibb's free energy for $B3$ and $B1$ phases with pressure and normalized volume with pressure and temperature
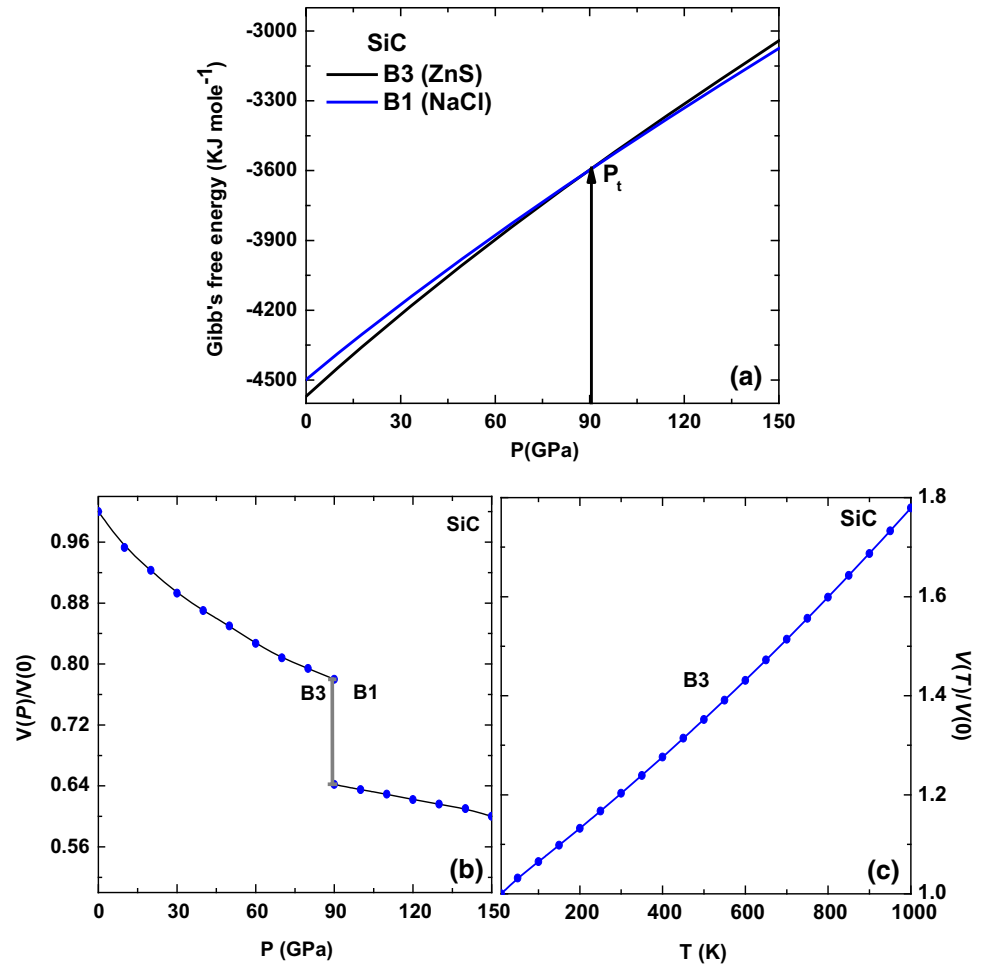
formulating interatomic potential to ensure whether long range or short-range interactions are at the origin of the structural transition. The many body force parameter as charge transfer $f(r)$ is positive as seen in Table 1. It is attributed to the fact that the charge transfer parameter is computed from the difference of second-order elastic constants C_{12} and C_{44}. The Cauchy energy $C_{12} - C_{44}$ is negative for SiC. Thus, consistent results lead to a test of the validity of assumptions made in model potential for SiC.

SiC shows a crystallographic transition from $B3$ to $B1$ in certain pressure range. Table 2 illustrates the computed phase-transition pressure (P_T) and compared with available experimental data [3, 4] and theoretical results [5–12, 14–16]. P_T for SiC is consistent with the experimental and other reported values and is attributed to proper formulation of interatomic potential, which considers the various interactions, explicitly the non-central many body forces as charge transfer interactions and covalency effects, as well as use of materials parameter based on experimental data. We may comment that any computational technique has its

own limitations related to the chosen materials basic parameters, basic sets, as well the accuracy and precisions used apart from the approximations laid in the method. Needless to suggest that there is always a variation in estimated parameters by each technique.

The values of relative volumes associated with various compressions are estimated from [51]

$$\frac{V_P}{V_0} = \left(1 + \frac{B'}{B_0}P\right)^{-1/B'}, \tag{19}$$

Here, V_0 (B_0) is the cell volume (bulk modulus) of SiC at ambient conditions and V_P is at finite pressure. The symbol B' is the pressure derivative of the bulk modulus. Figure 1b documents the estimated value of pressure-dependent radius for both $B3$ and $B1$ structures, the curve of volume collapse (V_P/V_0) with pressure to show phase diagram for $3C$ SiC. The phase diagram will let us estimate the magnitude of the discontinuity in volume at the transition pressure. The value of relative volumes is shown in Table 2. It is also compared with various experimental [3, 4] and other theoretical works [5–9, 11–14, 16].

Table 2 Calculated transition pressure P_T (GPa), volume collapse (%), aggregate second-order elastic constants (C_{11}, C_{12} and C_{44}), aggregate bulk modulus (B_T), (all are in 10^{10} Nm^{-2}) and pressure derivatives of SOECs (dB_T/dP, dC_{44}/dP and dC_S/dP) for Silicon Carbide in $B3$ phase

Property	Present	Expt.	FP LMTO	LDF	LDA	MD	DFT
Transition pressure P_T	90.0	100 [3],			66 ± 5 [5, 11]	100 [8]	66.6 [16]
		105 ± 4 [4]			63 [6]	90 [10, 15]	100 [7, 14]
							75.4 [9]
Volume collapse	13.8	20.3 [3]			18.5 [5, 11]	21 [8]	18.5 [16]
		15 ± 3 [4]					12 [7, 14]
							18 [9]
C_{11}	37.11	39.0 [47]	42.0 [51]		44.9 [62, 64]	39.0 [8]	41.51 [9]
		36.3 [56]	35.23 [58]		43.6 [63]	39.0 [10, 15]	37.1 [56]
C_{12}	22.34	14.2 [47]	12.6 [51]		14.6 [62, 64, 65]	14.4 [8]	13.19 [9]
		15.4 [56]	14.04 [58]		12.0 [63]	14.26 [10, 15]	16.9 [56]
C_{44}	27.93	25.6 [47]	28.7 [51]		25.6 [62, 64, 65]	17.9 [8]	26.54 [9]
		14.9 [56]	23.29 [58]		25.5 [63]	19.11 [10, 15]	17.6 [56]
B_T	27.30	22.7 [46]	22.3 [51]	24.9 [34]	21.2 [5, 11]	22.5 [8]	23.5 [7, 14]
		22.4 [59]	21.1 [58]	22.5 [61]	22.5 [62–65]	22.52 [10, 15]	22.71 [9]
		22.5 [60]					20.0 [57]
							22.5 [56]
C_S	7.38						
dB_T/dP	5.188	3.57 [46]	3.8 [51]	3.2 [62, 64, 65]	3.7 [5, 11]	5.5 [10, 15]	3.79 [9]
							7.3 [57]
dC_{44}/dP	5.198						
dC_S/dP	−0.0716						

Compressions in SiC at higher pressure indicate the mechanical stiffening of lattice.

Figure 1c discerns the variation of V_T/V_0 as functions of temperature in $B3$ phase. Here, V_T symbolizes the volume at various temperatures and V_0 at zero temperature and zero pressure volumes, respectively. A steep increase in the ratio V_T/V_0 with increasing temperature infers expansion of SiC lattice and is susceptible to temperature. On the other hand, SiC is compressed at higher pressures as shown in Fig. 1b. Henceforth, SiC lattice is thermally softened and mechanical stiffened. The normalized volume V_T/V_0 dependences on temperature are not known for SiC, but the present behaviour is consistent with available experimental [52] and theoretical [53] data on Li$_2$O.

The response of any material that undergoes stress, deforms and then recovers and returns to its original shape after stress ceases leads to the determination of elastic properties. The elastic properties are vital in generating information about the binding characteristic between adjacent atomic planes, anisotropic character of binding and structural stability. Apart from the structural stability of SiC in ZnS ($B3$) and NaCl ($B1$) structures, we now compute the aggregate elastic constants at normal and under hydrostatic pressure. Deduced values are documented in Table 2.

Using the stress–strain coefficients, one determines the second-order aggregate elastic constants C_{ij} under hydrostatic pressure with respect to finite strain. Also, proper parametrization of Coulomb, non-central many body forces, overlap repulsion, van der Waals interactions and zero point energy terms are essentially required.

The cubical symmetry of SiC dealt with three independent elastic constants C_{ij}. C_{11} is a response of resistance to deformation by a stress applied on (1,0,0) plane with polarization in the direction <100>. C_{11} probes elasticity in length and a longitudinal strain produces a change in C_{11}. C_{44} refers to the measurement of resistance to deformation with respect to a shearing stress applied across the (100) plane with polarization in the <010> direction. C_{12} and C_{44} are related to the elasticity in shape, which is a shear constant. A transverse strain causes a change in shape without a change in volume and hence C_{12} and C_{44} are less sensitive of pressure as compared to C_{11}.

The variation of three independent second-order aggregate elastic constants (SOECs): C_{11}, C_{12}, and C_{44} with external pressure for SiC in $B3$ and $B1$ phase is first discussed. As seen from Fig. 2a that C_{11} and C_{12} increase with increase in pressure in both $B3$ and $B1$ phases. Also, C_{44} decreases with the increase of pressure away from zero till the phase-transition pressures and then increases in $B1$

Fig. 2 Variation of aggregate second-order elastic constants (C_{ij}) with pressure and temperature
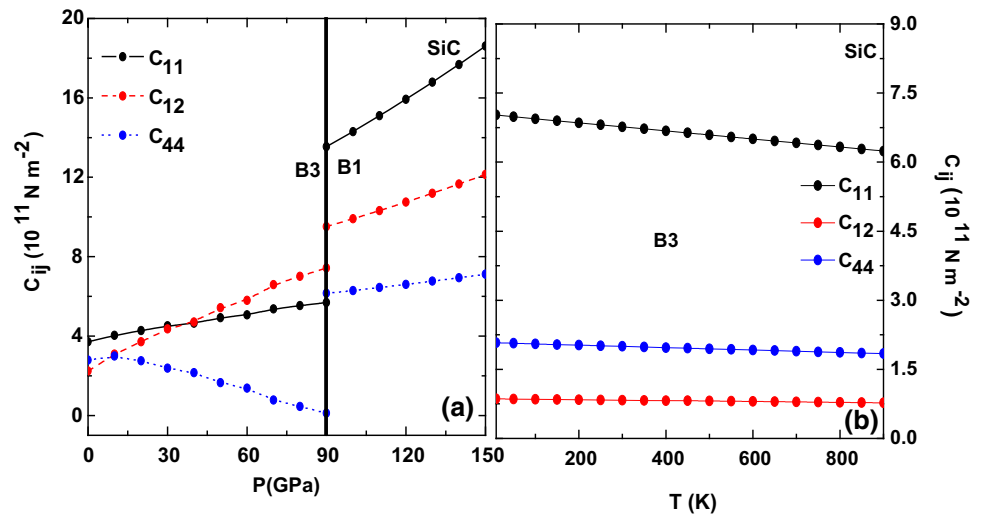
phase. Similar observations have earlier been reported in SiC [9, 10, 15]. A crossover of C_{12} and C_{44} in CaS has also been reported [54]. At phase transition pressures, SiC has witnessed a discontinuity in aggregate second-order elastic constants C_{ij}, which identifies the first-order phase transition. Thus, the proposed interaction potential incorporating charge transfer interactions ions of Si and C atom and covalency effects caused by Si–Si, Si–C, and C–C bonds consistently explains the high-pressure elastic behaviour.

The variations in C_{ij} with temperatures (T) for 3C SiC ceramics are plotted in Fig. 2b. It can be seen that the aggregate elastic constants C_{ij} (T) decrease linearly with the temperature in ZB phase. We note that the pressure dependence of aggregate elastic constants C_{ij} (P) documents an increasing trend (please see Fig. 2a). The physical interpretation of temperature dependence of C_{ij} showed that (a) values of C_{11} decrease more steeply with enhancing temperature, (b) C_{12}, and C_{44}, are less sensitive to temperature for 3C SiC ceramics, (c) C_{11} is remarkably larger than C_{12}, and C_{44}, and (d) values of all aggregate elastic constants C_{ij} are influenced by temperature dependence indicating that anharmonicity is substantial. Deduced values of C_{ij} with temperatures (T) are documented in Table 3 along with the available data on SiC at room temperature [55]. From the second-order aggregate elastic constants pressure and temperature-dependent behaviour, we comment that SiC lattice is mechanical stiffened and thermally softened.

Born criterion for a lattice to be mechanically stable infers that the elastic energy density must be a positive definite quadratic function of strain. The principal minors (alternatively the eigenvalues) of the elastic constant matrix should all be positive at ambient conditions. The mechanical stability conditions for a crystal suggest that elastic constants of a cubic crystal are as follows [29],

$$B_T = (C_{11} + 2C_{12})/3 > 0, \tag{20}$$

$$C_{11}, C_{44} > 0, \tag{21}$$

and

$$C_S = (C_{11} - C_{12})/2 > 0. \tag{22}$$

Here, C_{ij} are conventional aggregate elastic constants and B_T is bulk modulus. We represent, C_{44} and C_S as the shear and tetragonal moduli of a cubic crystal.

Table 2 illustrates the computed values of bulk modulus (B_T), shear moduli (C_{44}) and tetragonal moduli (C_S) which validates the elastic stability criteria for 3C SiC in $B3$ phase. The second-order elastic constants critically depend upon pressure leading to $C_{12} - C_{44} \neq 0$. The mechanically stable phases for cubic crystal satisfy the Born criteria: $C_{12} - C_{44} > 0$. The validity of above is readily seen by referring to Eqs. 51 and 52 for C_{12} and C_{44}. The equilibrium condition leads to $B_1 + B_2 = -1.261Z_m^2$ with emphasis on charge transfer interactions as well as covalency effects. For optimized values of r_i (r_j) the Cauchy discrepancy $C_{12} - C_{44}$ is nonzero at zero pressure and at zero temperature. It is also valid when the many body noncentral forces are not involved in long-range forces. The short-range and long-range effects are naturally of similar order of magnitude. This is due to the fact C_{ij} are calculated at optimized values of equilibrium distances rather than at experimental values.

Table 2 illustrates the calculated values of pressure derivatives of aggregate second-order elastic constants (dB_T/dP, dC_{44}/dP and dC_S/dP). These are compared with available experimental [46, 47, 56] and theoretical studies [8–10, 15, 46, 57–65]. For mechanical stability, the shear elastic constant C_{44} is nonzero and is known by combining mechanical stability with minimum energy conditions. The high-pressure stability also suggests that the stable phase of

Table 3 Calculated second-order elastic constant Cauchy discrepancy (Δ_1^2), anisotropy parameter (γ_i^2), isotropic shear modulus (G_H), Voigt's shear modulus (G_V), Reuss's shear modulus (G_R), Young's modulus (E), Poisson ratio (v), compressibility (β) and Gruneisen parameter (γ_G) of Silicon Carbide in $B3$ phase at zero pressure

Property	Present	Expt.	FP LMTO	LDF	LDA	MD	DFT
$\gamma_1^2(10^{10}\ \mathrm{Nm}^{-2})$	−0.736						
$\Delta_1^2\ (10^{10}\ \mathrm{Nm}^{-2})$	−5.588						
$G_H\ (10^{10}\ \mathrm{Nm}^{-2})$	16.47	19.2 [60]	21.9 [50]			12.37 [10, 15]	14.1 [56]
			16.9 [58]				
$G_V\ (10^{10}\ \mathrm{Nm}^{-2})$	19.71		23.1 [50]				14.6 [56]
			18.2 [58]				
$G_R\ (10^{10}\ \mathrm{Nm}^{-2})$	13.22		20.8 [50]				13.6 [56]
			15.7 [58]				
$E\ (10^{10}\ \mathrm{Nm}^{-2})$	41.22	44.8 [60]	49.60 [50]		56.7 [62, 64, 65]	31.36 [10, 15]	35.2 [56]
			40.1 [58]		55.0 [62, 64, 65]		
v	0.249	0.267 [47]	0.146 [50]			0.268 [10, 15]	1.0 [5, 11]
		0.168 [60]	0.201 [58]				0.259 [56]
$\beta\ (10^{-11}\ \mathrm{Pa}^{-1})$	0.024						0.1518 [5, 11]
γ_G	1.015			1.01 [61]	1.12 [5, 11]		

Fig. 3 Variation of Cauchy discrepancy (Δ_1^2) and elastic anisotropy (γ_1^2) in second-order elastic constant (C_{ij}) with pressure
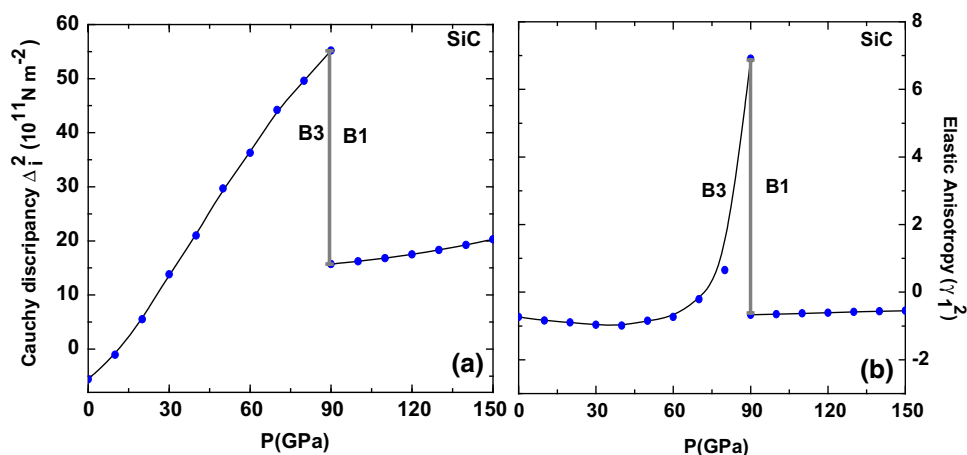
the crystal possesses the lowest potential energy among the mechanically stable lattices [66].

The elasticity in 3C SiC is thus probed by a non-central many body force potential which assumes that the interatomic forces have a certain shape and directionality. The Cauchy discrepancy is defined as $\Delta_1^2 = C_{12} - C_{44} - 2P$. Here, Δ_1^2 is a measure of the contribution from the non-central many body force. However, for pure central interatomic potentials, Cauchy relation is $C_{12} = C_{44} + 2P$.

At zero pressure, the Cauchy discrepancy (Δ_1^2) in SiC is about $-5.588 \times 10^{10}\ \mathrm{Nm}^{-2}$. The Δ_1^2 further enhances on increasing the pressure in both phases as depicted in Fig. 3a. In SiC, larger deviation of Δ_1^2 essentially points to the importance of the many body non-central (charge transfer and covalency) interaction in the interatomic

potential and anharmonic effects are substantial at high pressures. The strength of non-central many body forces incorporating charge transfer interactions and covalency effects is witnessed by significant deviation in Δ_1^2 at different pressures not only in ZB but also in RS structure, although weak. The importance of many body non-central forces and anharmonic effects is further explored by analysing the higher order elastic constants explicitly the third-order elastic constants. Usually, the anharmonic effects are noticeable at high pressure as reflected from elastic constants behaviour.

The anisotropy in second-order elastic constants is reflected from geophysical activities of various materials and alloys. The anisotropic parameter γ is unity for isotropic elasticity. As far as cubic crystal is concerned,

although it is isotropic in structure, it has elastic anisotropy other than unity. This is a consequence of fourth rank tensor property of elasticity.

We define elastic anisotropic parameter γ_1^2 in terms of aggregate C_{ij} as [67]:

$$\gamma_1^2 = \frac{C_{11} - C_{12} - 2C_{44}}{2C_{44}} \qquad (23)$$

The pressure dependence of the elastic anisotropic parameter γ_1^2 in SiC is shown in Fig. 3b. It is evident that γ_1^2 in SiC is insensitive below transition pressure and also at low pressures. A jump has been noted at P_T (=90 GPa) inferring first-order structural phase transition. Furthermore, γ_1^2 in SiC remains unaltered for B1 phase for higher pressures. The value of anisotropic parameter γ_1^2 for SiC is given in Table 4 at $T = 0$ K and $P = 0$ GPa.

During mechanical processing, explicitly in fabrication the melting ranges of materials and alloys are substantial. The usage of an alloy in the applications as the success of the melting and casting operations depends on the correct selection of temperature. Once solidified and primary processed (rolling or forging), the melting temperature has little significance to designers, engineers and users. The melting temperature influences elevated temperature

Table 4 Calculated aggregate second-order elastic constants (C_{11}, C_{12} and C_{44}) and aggregate bulk modulus (B_T), second-order elastic constant anisotropy parameter (γ_i^2), isotropic shear modulus (G_H), Voigt's shear modulus (G_V), Reuss's shear modulus (G_R), Young's modulus (E), Poisson ratio (v), First and second Lame constant (λ, μ), longitudinal (v_l), shear (v_s) and average elastic wave velocity (v_m), Kleinman parameter (ξ) and thermodynamical properties: Debye temperature (θ_D) of silicon carbide in B3 phase at temperature of about 300 K

Materials parameter	SiC
C_{11} (10^{10} Nm^{-2})	67.65, 35.23 [49]
C_{12} (10^{10} Nm^{-2})	8.31, 14.04 [49]
C_{44} (10^{10} Nm^{-2})	19.99, 23.29 [49]
B_T (10^{10} Nm^{-2})	28.1
C_S (10^{10} Nm^{-2})	29.7
G_H (10^{10} Nm^{-2})	23.43
G_V (10^{10} Nm^{-2})	23.86
G_R (10^{10} Nm^{-2})	22.99
E (10^{10} Nm^{-2})	54.9, 43.7 [71]
v	0.174, 0.167 [71]
λ (10^{10} Nm^{-2})	12.47
μ (10^{10} Nm^{-2})	23.43
v_l (ms^{-1})	12,440, 12,182 [71]
v_s (ms^{-1})	7819, 7701 [71]
v_m (ms^{-1})	1824
ξ	0.274
θ_D (K)	708.60

properties, such as creep strength, but the researchers have limited interest. The pressure dependence of the melting temperature: $T_M = 553$ K $+ 5.91 C_{11}$ K GPa^{-1} for SiC in B3 and B1 phase is discerned in Fig. 4. It is noticed that T_M enhances with increased pressure or in other words the resistance to deformation by a stress increases. It is noticed that at zero pressure, the melting temperature of SiC is 2746 K consistent with reported value of about 3100 ± 40 K [1, 2]. At P_T (=90 GPa), its value is about 4000 K which enhances further in B1 phase. An increase in T_M with variations in pressure infers the hardening or stiffening of the lattice. Higher melting temperature symbolizes higher shear modulus (G), and Young's modulus (E) values that we shall see later on. The data on its melting under high pressure are very limited and extremely contradictory, which does not allow one to make any conclusions about congruent or incongruent melting behaviour as well as the slope of the melting curve of SiC.

SiC is the only compound in the Si(IV)–C(IV) binary system and is obtained by electromelting high purity silica sand with petroleum coke, also of good quality. This melting takes place at high temperature about 2473 K and requires a large quantity of energy to produce. It also requires energy for it to dissociate into about 2/3 Si and 1/3 C in the induction furnace [1, 2]. The better quality raw materials produce better quality SiC, which is lower in nitrogen, sulphur, hydrogen and other trace elements. Figure 4 shows the temperature dependence of the melting temperature for SiC estimated from the C_{11} elastic constant as discussed previously. At room temperature its value is about 4550 K which drops and is 4200 K at 1000 K in B3 phase. The suppressed T_M with increased temperature indicates that there is a decrease in the resistance to deformation by a stress induced due to temperature. The suppressed T_M infers the weakening of the lattice as a result of thermal softening. Usually, SiC does not melt, it actually dissolves since its melting point is about 2973 K. Its behaviour in the molten metal is similar to sugar dissolving in coffee. This aspect is very important for the use of SiC.

For cubic lattice, three second-order elastic constants and the six non-vanishing third-order elastic constants are obtained from crystal geometry. The anharmonicity of a crystal lattice is successfully probed in terms of higher order elastic constants. The third-order terms in the strain variables are deduced from derivatives of elastic energy (please see Appendix for both ZB B3 and RS B1 phases). For SiC, the third-order aggregate elastic constants C_{111}, C_{112}, C_{166}, C_{144}, and C_{456}, are negative and only C_{123} is positive at $P = 0$ GPa i.e., in B3 phase. We note that no such efforts have been made in the past for third-order elastic constants of SiC. Thus, deduced information on pressure-dependent C_{ijk} will serve as a guide line for future

Fig. 4 Variation of melting temperature (T_M) with pressure and temperature

research and its application in materials technology. This information is useful as the structural strengths of a material are successfully known from the knowledge of elastic constants. The microstructures developed on the applied pressure and temperature can be known from third-order elastic constants variations.

The variation of aggregate third-order elastic constants (TOECs) with pressure for SiC in B3 and B1 phase is sketched in Fig. 5. For SiC in cubic phase, the C_{144}, and C_{166} increases with enhancing pressure. Other TOECs as C_{456}, C_{112}, C_{111}, and C_{123} infer a decreasing trend. We note that C_{144} is remarkably larger as compared to other TOECs. Furthermore, aggregate elastic constants C_{ijk} inferring the anharmonic effects are influenced by application of pressure in SiC. In the present interatomic potential, C_{ijk} are affected by the inclusion of second-nearest-neighbour interaction and are influenced by the short-range interactions (please see Eqs. 60–65 in the Appendix). Also, many body non-central forces as long-range Coulomb, charge transfer interactions and covalency are effective in SiC. We comment that pressure-dependent C_{ijk} behaviour can have a direct means to describe the interatomic forces at high pressure. It successfully cares the short-range forces, and a balance between long range and short-range forces.

As a next step, we intend to study the anisotropy among C_{ijk}. The equilibrium condition in the interatomic potential infers $B_1 + B_2 = -1.261 \, Z_m^2$. The Cauchy discrepancy Δ_i^3 among third-order elastic constants are: (a) $\Delta_1^3 = C_{112} - C_{166} - 2P$; (b) $\Delta_2^3 = C_{123} - C_{456} - 2P$; (c) $\Delta_3^3 = C_{144} - C_{456} - 2P$; and (d) $\Delta_4^3 = C_{123} - C_{144} - 2P$. The C_{ijk} at zero pressure i.e., in B3 phase are influenced by contributions from both long-range and short-range interactions. Henceforth, Δ_i^3 is an indicator of the contribution from the non-central many body force. Figure 5a shows the variation

of Δ_i^3 as functions of pressure. The significant deviation in Δ_i^3 is a natural consequence of the non-central many body forces as charge transfer interactions ions of Si and C atom and covalency effects caused by Si–Si, Si–C, and C–C bonds apart from short-range interactions as the induced charge dipole–dipole and charge dipole–quadruple (van der Waals) interaction and the overlap repulsion. At zero pressure, Δ_2^3 and Δ_3^3 are positive, while to that Δ_1^3 and Δ_4^3 are negative in B3 phase. A growth in Δ_2^3 and Δ_3^3 and decay in with enhanced pressure is witnessed with enhanced pressure till phase transition pressure. However, all Δ_i^3 is negative in B1 phase indicating the importance of non-central many body forces and anharmonic effects in SiC ceramics. As far as we know, there are no experimental results available for Cauchy discrepancy Δ_i^3 in SiC.

For cubic crystal structures, the aggregate third-order elastic constants C_{ijk} discern three anisotropy coefficients and three isotropic coefficients. It is useful to express linear combinations of the anisotropy coefficients and dividing them by the isotropic coefficients [68–70]. The anisotropy coefficients γ_i^3 are as follows:

$$\gamma_1^3 = \frac{3C_{112} - C_{111} - 12C_{144} + 12C_{166} - 16C_{456} - 2C_{123}}{2C_{123}} \tag{24}$$

$$\gamma_2^3 = \frac{C_{111} - C_{123} - 2C_{144}}{2C_{144}} \tag{25}$$

$$\gamma_3^3 = \frac{C_{166} - C_{144} - 2C_{456}}{2C_{456}} \tag{26}$$

The pressure dependence of the elastic anisotropic parameter γ_i^3 for both phases is sketched in Fig. 5b. The elastic anisotropy (γ_2^3 and γ_3^3) in B3 phase is less sensitive. On the other hand, γ_1^3 shows variation with increase in pressure in B3 phase. The anisotropy factor γ_1^3 is negative and shows a

Fig. 5 Variation of aggregate third-order elastic constants (C_{ijk}) with pressure, Cauchy discrepancy (Δ_i^3) and elastic anisotropy (γ_i^3) in third-order elastic constant with pressure
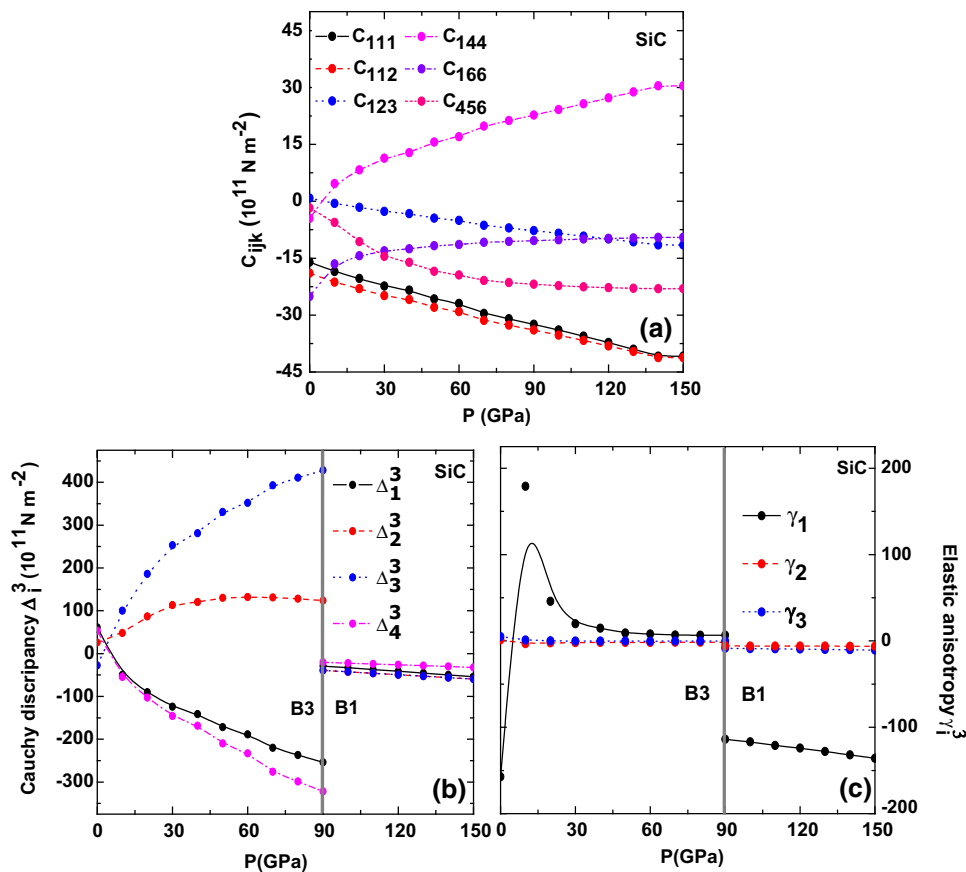
decreasing trend with pressure in $B1$ phase at higher pressures. Values of γ_i^3 are given in Table 5 at zero temperature and pressure. As far as we know, there are no experimental and theoretical results available for comparison.

The strength and hardness are key issues for materials useful in technological applications. The mechanical strength and hardness of SiC can be known once elastic constants are known. We now determine elastic moduli at various pressures of SiC which are of substantial importance in engineering, geophysical and seismological application. The elastic properties are important in probing the bonding characteristic between adjacent atomic planes and the anisotropic character of the solid. Crystals leading to elasticity under application of pressure identify the response of a crystal under external strain. This valuable information is characterized by isotropic shear modulus (G_H), and Young's modulus (E). We note that hardness of polycrystalline materials is inhibited in elastic response as G_H and E.

The resistance to volume change and resistance to reversible deformations upon applied pressures are accounted by Voigt–Reuss–Hill approximation using G_H and E following [68–70]:

$$G_H = \frac{G_V + G_R}{2} \tag{27}$$

Herein, G_V (G_R) is Voigt's (Reuss's) shear modulus corresponding to the upper (lower) bound of G_H values. The G_V (G_R) is obtained from C_{ij} assuming uniform strain throughout the sample as

$$G_V = \frac{C_{11} - C_{12} + 3C_{44}}{5} \tag{28}$$

and

$$\frac{5}{G_R} = \frac{4}{(C_{11} - C_{12})} + \frac{3}{C_{44}} \tag{29}$$

Hardness of materials is usually measured in terms of isotropic shear modulus (G_H), and Young's modulus (E) or bulk modulus (B_T). The bulk modulus infers resistance to volume change by applied pressure. The isotropic shear modulus (G_H) measures the resistance to reversible deformations upon shear stress. In such a situation, G_H is a better probe to measure hardness than the bulk modulus (B_T). Table 4 illustrates the calculated isotropic shear modulus (G_H), Voigt's shear modulus (G_V) and Reuss's shear modulus (G_R) for SiC ceramics at zero temperature and

Table 5 Calculated aggregate third-order elastic constant (C_{ijk}), third-order elastic constant anisotropy parameter (γ_i^3), First and second Lame constant (λ, μ), longitudinal (v_l), shear (v_s) and average elastic wave velocity (v_m), Kleinman parameter (ξ) thermodynamical properties: force constant (f), Reststrahlen frequency (v_o), Debye temperature (θ_D), and average elastic constant (C), of Silicon Carbide in $B3$ phase at zero pressure

Materials parameter	SiC
C_{111} (10^{10} Nm^{-2})	-160.70
C_{112} (10^{10} Nm^{-2})	-189.70
C_{123} (10^{10} Nm^{-2})	8.33
C_{144} (10^{10} Nm^{-2})	-44.85
C_{166} (10^{10} Nm^{-2})	-250.90
C_{456} (10^{10} Nm^{-2})	-17.38
γ_1^3	-157.283
γ_2^3	1.207
γ_3^3	4.927
λ (10^{10} Nm^{-2})	16.29
μ (10^{10} Nm^{-2})	16.47
v_l (ms^{-1})	$12{,}400$
v_s (ms^{-1})	7172
v_m (ms^{-1})	1688
ξ	0.709
f (10^5 dyne cm^{-1})	7.187
v_0 (10^{12} Hz)	6.867
θ_D (K)	611.758
$C_{av.}$ (10^{10} Nm^{-2})	22.82

pressure along with a comparison with the available theoretical results [10, 15, 50, 56, 58, 60].

A decreasing and then increasing nature of the isotropic shear modulus G_H, G_V and G_R is witnessed in $B3$ phase of SiC. On the other hand, a steep increase in G_H, G_V and G_R is seen with enhanced pressure in $B1$ phase at higher pressures as plotted in Fig. 6a. The explanation of the above characteristics lies in a fact that both G_V and G_R are influenced by aggregate elastic constant C_{44}. Thus, G_V decreases as C_{44} decreases with enhanced pressure in ZnS phase. On the other hand, Reuss's shear modulus (G_R) pressure-dependent behaviour is integrated by combination of $C_{11} - C_{12}$ pressure-dependent behaviour as well as to that of C_{44} pressure-dependent behaviour. G_R initially decreases and then starts increasing at about 30 GPa and is attributed to steep decrease in C_{44}. We end up by stating that above transition pressure an increase in G_H, G_V and G_R support our earlier prediction about mechanical stiffening of lattice.

The high temperature studies of materials at ambient pressure lead to the performance of a material in terms of (a) the understanding of vibrational anharmonicity that is associated with the relative interplay of long-range and short-range potential energy function, (b) thermal response

in terms of softening or hardening and (c) the elastic behaviour of materials as the elasticity, extensibility, acoustic transmission velocity, Debye temperature, specific heat, and thermal conductivity.

The high temperature investigations cause laboratory difficulties and structural changes make the phenomenon more amenable to interpretation. Figure 6b displays the G_H, G_V and G_R behaviour of 3C SiC ceramics as functions of temperature (at zero pressure). We note that the isotropic shear modulus of SiC is decreasing with enhanced temperature. The steep decrease of G_H, G_V, and G_R is in accordance with aggregate second-order elastic constant C_{ij} behaviour with temperature. Suppressed G_H, G_V and G_R as functions of temperature infer the weakening of the lattice as a result of thermal softening.

The tensile modulus as Young's modulus (E) further elaborates the stiffness property. E is also defined in terms of Reuss's shear modulus (G_H), and bulk modulus (B_T):

$$E = \frac{9G_H B_T}{G_H + 3B_T} \tag{30}$$

The tensile strength as Young's modulus (E) for 3C SiC is illustrated in Table 4 for ZnS ($B3$) phase along with a comparison with the reported data [10, 15, 50, 55, 56, 60, 62, 64, 65]. The model calculations presented here lead to E value of about 411 GPa at zero pressure. It is known that the material is stiffer if its Young's modulus is high [E of steel, graphene and diamond is ~ 200, 1000 and 1220 GPa]. As inferred SiC is less stiff as compare to graphene and diamond. The pressure dependence of the Young's modulus (E), of SiC is sketched in Fig. 7a. A decreasing trend of E in $B3$ phase infers the weakening of tensile strength till 90 GPa and an increasing trend of E in $B1$ phase essentially identifies more stiffening. Looking to the wide usage of SiC in gas turbines, heat exchangers, ceramics fans, radar, microwave, solar cell, and high-voltage devices, these properties are worth investigating.

Figure 7b illustrates the temperature dependence of the tensile strength as Young's modulus (E) for 3C SiC ceramics. A decreasing trend is inferred with increase in temperature. Matsumoto and researchers have reported the Young's modulus and Poisson's ratio of SiC ceramics at temperatures >1400 °C using laser ultrasonics coupled with Fabry-Pérot interferometry as well ultrasonic pulse method [71]. It is reported that E is about 438 GPa at $T = 273$ K and shows a decreasing behaviour with increasing temperature. The model calculations presented here lead to a value of about 549 GPa at room temperature which is comparable to reported E of 437 GPa for 3C SiC ceramics [71]. A reduction of E with temperature is a signature of bond weakening or thermal softening.

We now make a comparison of tensile strength E (P) and E (T) of 3C SiC ceramics. It is noted that

Fig. 6 Variation of Isotropic shear modulus (G_H, G_V and G_R) with pressure and temperature
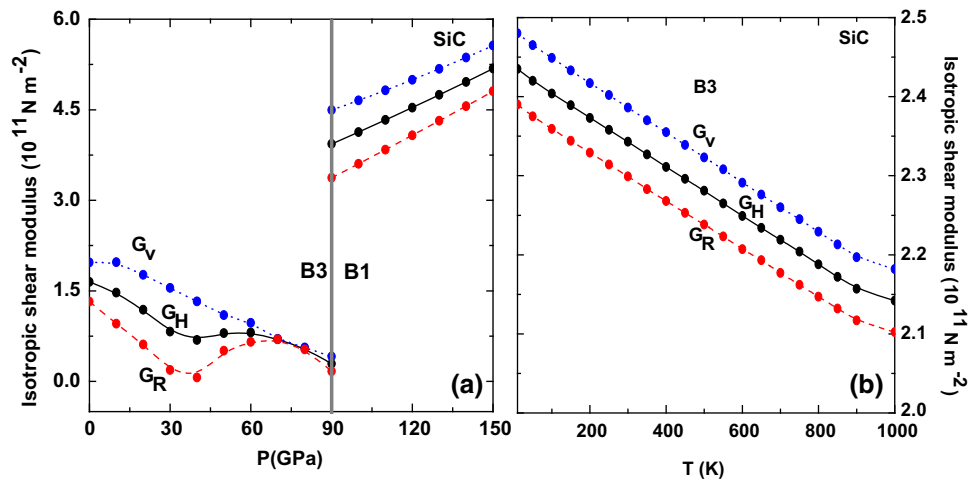
Fig. 7 Variation of Young's modulus (E) with pressure and temperature
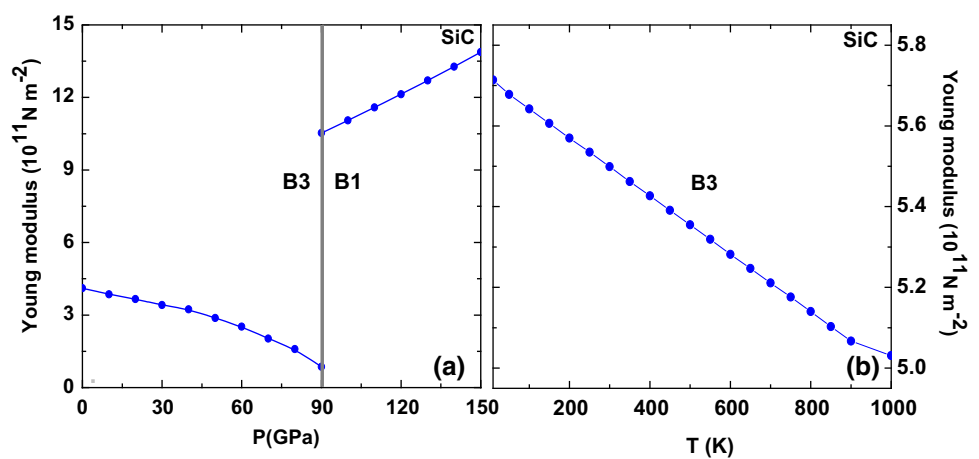
E (P) values are smaller than E (T) for SiC at low pressures and temperatures. It implies that E (P) and E (T) are although susceptible to external variables as pressure and temperature, but it is their Si and C ions in 3C SiC ceramics that makes SiC lattice to be mechanical hard due to bond strengthening and thermal soft due to bond weakening. It is worth commenting that while tailoring the composites based on SiC, one should seek its performance in terms of tensile strength.

Another interest in 3C SiC is to probe the ductile and brittle nature of Silicon and Carbon-based alloys are important and predicted from the knowledge of second-order elastic constants. Ductile materials as Steel and aluminium sustain large strains before rupture, while to that brittle materials as glass and cast iron fractured at lower strains. For materials design and advances in metallurgy as well composite technology, the materials response for applied pressures and temperatures are often gauzed by stress–strain characteristics. Composites are predictive as depending on the external variable (pressure and temperature), the response of the constituent element is tailored in

terms of ductile or brittle nature. Also ductile element in composites may become brittle as the pressure or temperature is increased or decreased. Once the pressure dependence of shear modulus (G_H), and Young's modulus (E) or bulk modulus (B_T) is known, it is worth investigating ductile and brittle nature of SiC.

The shear modulus (G_H,) measures the resistance to plastic deformation, while the bulk modulus (B_T) probes the resistance to fracture. An empirical relation in terms of the ratio of these moduli is known to differentiate ductile and brittle nature. In accordance with the Pugh's ratio ϕ (=B_T/G_H) > 1.75, the material sustains large strains before rupture *i.e.*, the ductile response. On the other hand, for $\phi \leq 1.75$ the material is brittle. Empirically, 1.75 is a critical value that separates ductile and brittle response of materials [72].

In Fig. 8a, we have shown the Pugh ratio ϕ as functions of pressure. Note that SiC is ductile in ZnS phase (at zero as well at low pressures). Brittle nature is noticed at higher pressures in ZnS phase. Furthermore, brittle response of SiC is also noticed in rock salt structure. Hence, ceramics SiC is ductile/brittle irrespective of any structural

transformations. To our knowledge, perovskite are ductile/brittle that is a test for its deformation before fracture. In materials performance ductility is a powerful probe for quality control. It provides a means to assess the level of impurities and proper processing of a material. Hence, we classify 3C SiC as brittle material at higher pressures and ductile at zero pressure on the basis of Pugh ratio. The magnitude of elastic constants and shear moduli agrees with ductility degree of SiC in both B3 and B1 phase.

The Poisson's ratio is another measure to differentiate the ductility and brittleness of materials [73]. The critical value of Poisson's ratio (in terms of B_T and G_H) v is 0.33 that separates ductile and brittle nature of any material. If $v > 0.33$, the material is ductile, and for $v < 0.33$, the brittle response of material is observed such as ceramics. However, Poisson's ratio lies in between -1.0 and 0.5 which are the lower and upper bounds. The lower bound is a signature of the response of the materials that do not change its shape and the upper bound indicates that the volume is unchanged. The Poisson's ratio v in terms of bulk modulus B_T and the shear modulus G_H is expressed as [68–70],

$$v = \frac{1}{2}\left[3\frac{B_T}{G_H} - 2\right]\left[3\frac{B_T}{G_H} + 1\right]^{-1} \tag{31}$$

Figure 8a summarizes the pressure-dependent results of Poisson's ratio v. SiC in ZnS phase documents mixed behaviour. At zero pressure ($P = 0$ GPa), the value of v is about 0.25 for SiC. At lower pressures, SiC is brittle, above 15 GPa and till phase transition pressure, ductile nature of SiC is observed. Above P_T (=90 GPa), the value of v is about 0.34 for B1 phase. Above P_T, at higher pressures, in the RS structure, SiC remains brittle with increasing pressure. Deduced value of v is in good agreement with available experimental and theoretical results [5, 10, 11, 15, 47, 50, 56, 59, 63]. As per definition of Poisson's ratio, 3C SiC is brittle. It should be pointed out here that both Pugh (SiC as ductile) and Poisson's ratio (SiC as brittle)

give contradictory results. The two empirical rules only differ on the exact border between the two types of behaviour. In view of this, the pressure-dependent variations of SiC allow it to consider as a borderline case between the classes of ductile and brittle materials. We note the ceramics are brittle, but perovskites are ductile.

The Poisson's ratio v behaviour as a function of temperature is sketched in Fig. 8b. The Poisson's ratio v is independent of temperature and is consistent with the earlier measured v by laser ultrasonics method [71]. Beginning from zero temperature and at high temperatures in ZB phase, $v \approx 0.174$ is obtained for 3C SiC. The temperature-dependent Poisson's ratio reflects brittle nature of SiC, while to that a borderline case between the classes of ductile and brittle materials is known from pressure dependence. Poisson's ratio is thus an effective indicator to control the level of impurities and processing of SiC ceramics. For covalent materials, v is small ($v \sim 0.1$), whereas for metallic materials v is typically 0.33. It is worth mentioning that agreement with experimental and theoretical data is not fortuitous, but it is attributed to proper parametrization and formulation of potential with non-central many body forces as charge transfer interactions ions of Si and C atom and covalency effects caused by Si–Si, Si–C, and C–C bonds apart from short-range interactions as the induced charge dipole–dipole and charge dipole–quadruple (van der Waals) interaction and the overlap repulsion.

Usually, the elastic moduli describe only reversible response of a material to small strain near equilibrium. The intrinsic strength of a material reflects permanent plastic deformation at large shear strain. Consequently, to further understand the behaviour of SiC in terms of Vickers hardness: $H_V = 2 \ (\phi^2 G_H)^{0.585} - 3$. Here, $\phi = B_T/G_H$. Figure 9a illustrates the theoretical Vickers hardness as a function of pressure. It is clear from the plot that the Vickers hardness H_V decreases in B3 phase and then increases in B1 phase with increase in pressure, which

Fig. 8 Variation of Poisson's ratio (v) and Pugh's modulus ratio (Φ) with pressure and temperature
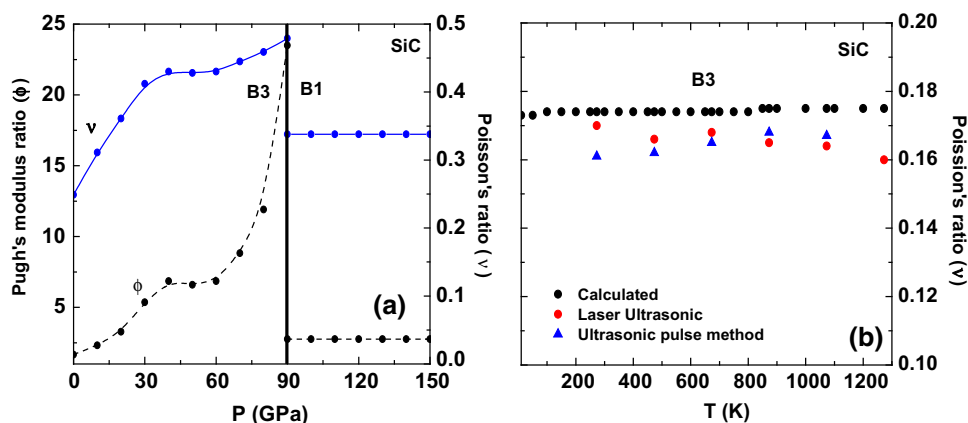
indicates that SiC becomes hard under pressure implying its good mechanical properties. Figure 9b shows Vickers hardness as a function of temperature for SiC. It is clear from the plot that the Vickers hardness H_V decreases in $B1$ phase, which indicates that SiC gets softened with enhanced temperature. Apart from the elastic anisotropy of crystals, the hardness is important to discuss their properties because it is highly correlated with the possibility of inducing microcracks in materials.

SiCs are promising materials with wide range of applicability's with effective mechanical properties. Usually, materials elastic properties are a source of valuable information where materials mechanics is significant as the knowledge of deformational characteristics of materials is essential in engineering design and construction of effective structures. Having, understood the materials elastic behaviour using Bulk modulus (B_T), shear modulus (G_H, G_V and G_R), and Young modulus (E), in the following, we will use our calculated elastic constants to discuss the compressional and shear wave velocity in ceramics SiC. The velocities of the longitudinal v_l and shear waves v_s are known from the Lamé's constants, λ and μ. The compressional wave with velocity v_l propagates back and forth in a crystal. The shear waves with velocity v_s go up and down.

The Lamé's constants are related to Young's modulus (E) and Poisson's ratio (v) [correlating the bulk modulus B_T and the shear modulus G_H]. The first Lamé's constant (λ) measures the compressibility of the material. The second Lamé's constant (μ) infers its shear stiffness [68–70]. The Lamé's constants (λ and μ) are expressed as:

$$\lambda = \frac{vE}{(1+v)(1-2v)} \tag{32}$$

$$\mu = \frac{E}{2(1+v)} \tag{33}$$

Figure 10a displays the pressure dependence of the first and second Lamé's constants (λ, μ). Starting from zero pressure and at high pressures, both Lamé's constants (λ, μ) are positive. Note that the Lamé's constant (λ) can be negative; however, for most materials it is also positive. The second Lamé's constant (μ) is positive. An increasing trend of compressibility (λ) of SiC is witnessed in terms of λ as seen in both ZB and RS structures and is attributed to mechanical hardening of lattice. The decreasing trend in $B3$ phase and increasing trend in $B1$ phase of shear modulus (G_H, G_V and G_R) results in a decreasing behaviour of shear stiffness (μ) in $B3$ phase and then enhanced shear stiffness in $B1$ phase. Note that λ and μ together constitute a parameterization of the elastic moduli for homogeneous isotropic media. The values of pressure-dependent Lamé's constants (λ, μ) are documented in Table 5. Deduced values of Lamé's constants (λ, μ) could not be compared due to lack of data on SiC. Figure 10b summarizes the temperature-dependent behaviour of Lamé's constants (λ, μ), for 3C SiC. It is noticed that both Lamé's constants (λ, μ) are decreasing with increasing temperature. Thus, both compressibility and shear stiffness showed decreasing trend with temperature variations and identifies once again the thermal softening of SiC.

The Lamé's constants (λ, μ) determine the longitudinal (shear) wave velocity as

$$v_l = \left[\frac{\lambda + 2\mu}{\rho} \right]^{\frac{1}{2}} \tag{34}$$

$$v_s = \left[\frac{\mu}{\rho} \right]^{\frac{1}{2}} \tag{35}$$

Here, ρ is the density. The average wave velocity v_m has been approximately given by

$$v_m = \left[\frac{1}{3} \left(\frac{2}{v_t^3} + \frac{1}{v_s^3} \right) \right]^{-\frac{1}{3}} \tag{36}$$

Fig. 9 Variation of Hardness (H_V) as a function of pressure and temperature
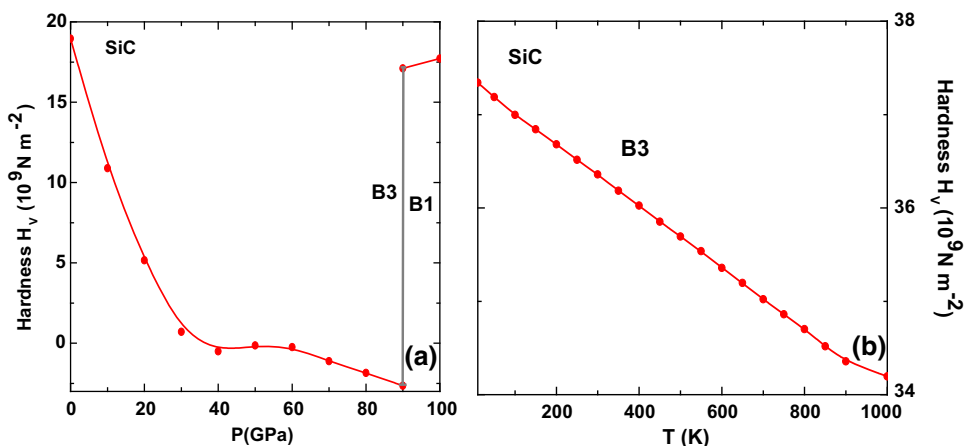
The compressional longitudinal (shear) wave velocity thus depends on density of the material as well on Bulk modulus (B_T), shear modulus (G_H, G_V and G_R), and Young modulus (E). We note that Bulk modulus (B_T) has a strong dependence on the density of the material, Young modulus (E) displays a weak dependence, while the shear modulus (G_H) is independent of density.

Figure 11a displays the pressure dependence of the longitudinal (shear) wave velocity in SiC. In ZB phase, beginning from zero pressures and at high pressures, compressional wave velocity v_l increases while to that shear wave velocity v_s decreases. Both compression and shear waves increase with enhanced pressure in $B1$ structure. Deduced values of longitudinal, shear and average elastic wave velocities propagating in SiC are illustrated in Table 5 at zero temperature and pressure. Figure 11b represents the temperature dependence of the longitudinal (shear) velocity, respectively. It is noticed that both longitudinal (shear) wave velocity decreases in $B3$ phase with enhanced temperature. The values of the longitudinal, shear and average elastic wave velocities propagating in $3C$ SiC ceramics are documented in Table 4 at room temperature. Deduced values of wave velocities are in good

agreement with the measured values by laser ultrasonics method [71]. The high temperature behaviour of longitudinal (shear) wave velocity for SiC can be considered as predictive studies as they cannot be compared due to unavailability of high temperature data.

The Navier's equation is also used to determine the longitudinal and the shear wave velocity [74, 75]. These are written in terms of Reuss's shear modulus (G_H), and bulk modulus (B_T) as

$$v_l = \left[\frac{3B_T + 4G_H}{3\rho} \right]^{\frac{1}{2}} \tag{37}$$

$$v_s = \left[\frac{G_H}{\rho} \right]^{\frac{1}{2}} \tag{38}$$

Elastic, plastic and molten state properties with pressure as controlling variable are useful for tailoring composites. The Lamé's constants (λ, μ) are of substantial interest for plastic materials. Referring to equations 32 and 33, we note that as the Poisson's ratio (ν) increases, the Lamé's constants (λ, μ) numerically approach the bulk modulus (E). For fluids, the Reuss's shear modulus (G_H) vanishes as the viscosity of the fluid approaches zero. The above is

Fig. 10 Variation of Lamé's constant (λ, μ) with pressure and temperature
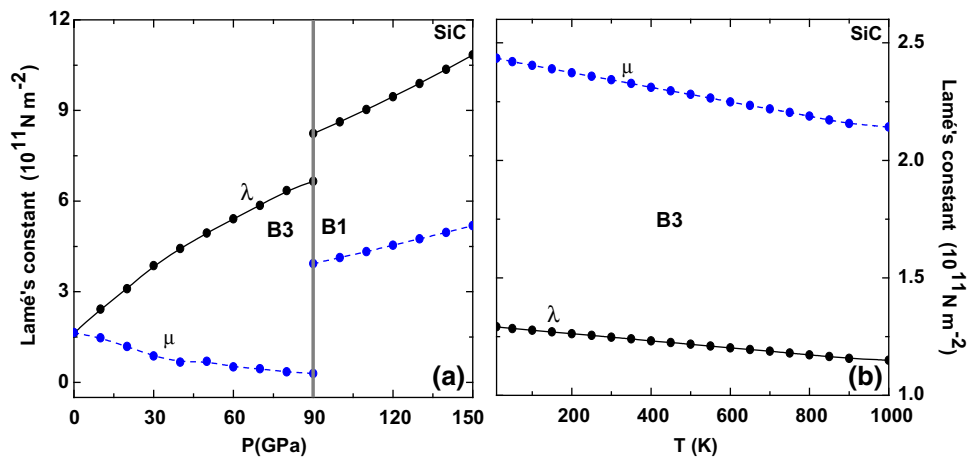
Fig. 11 Variation of elastic wave velocity v_l and v_s with pressure and temperature
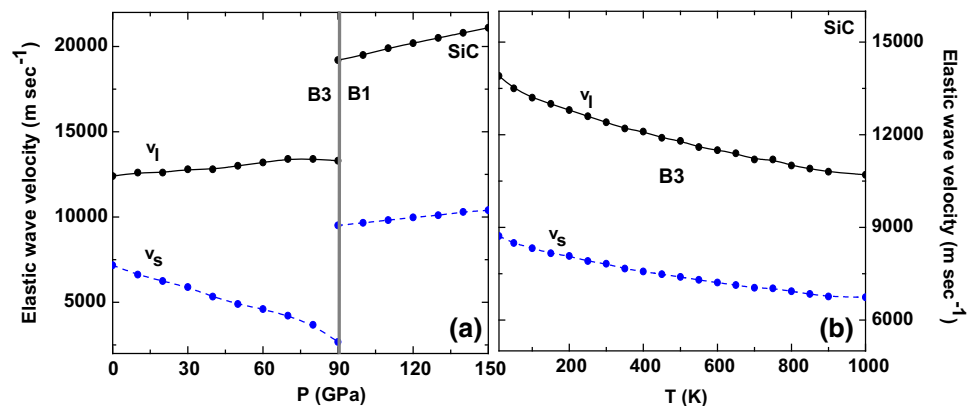
important in context of the present computation and can also be cross-checked from the relation between bulk modulus and Reuss's shear modulus: $B_T = \lambda + 2\,G_H/3$. Furthermore, G_H approaches zero for fluids and hence the Poisson's ratio is ~ 0.5.

The response to deformations against bond bending or bond-angle distortion is relevant for materials with promising technological applications and also a test to validate the many body non-central potential that we dealt with. The aggregate elastic constants infer the elastic properties of material that undergo stress, deform and then recover after returns to its original shape after stress ceases. The nature of elastic constants in solids holds a great importance to elucidate the microscopic nature interatomic bonding, equations of state, and vibrational density of states. The above can be understood in terms of Kleinman parameter, ξ, which describes the relative positions of the cation and anion sub-lattices under volume-conserving strain distortions for which positions are not fixed by symmetry [76, 77]. We have explored its applicability to ceramics SiC using [78].

$$\xi = \frac{C_{11} + 8C_{12}}{7C_{11} + 2C_{12}} \tag{39}$$

Deduced value of $\xi \approx 0.709$ is documented in Table 5 for 3C SiC at zero temperature and pressure. The value of $\xi \approx 0.274$ is obtained at room temperature and is reported in Table 4 for 3C SiC. A low value of ξ implies a large resistance against bond bending or bond-angle distortion and vice versa [79]. Thus, SiC shows resistance against bond bending or bond-angle distortion and hence is of immense use in heat exchangers and ceramics fans. As far as we know, there is no experimental result available for Kleinman parameter and is considered as a prediction study. For both ZB and RS structures, the knowledge of elastic constants at variable pressure is worth investigating aimed for practical applications related to the mechanical properties of a solid: load deflection, thermo elastic stress, internal strain, elastic wave velocities, and fracture toughness.

Physical properties as thermal expansion, heat capacity and Grüneisen parameter can be explained with higher order terms of the interaction potential. The thermal process in terms of heat conduction is hindered if one considers a solid to be perfectly harmonic and thermal conductivity will be infinitely large. Thus, the role of anharmonic effects or phonon decay is important as enhanced pressures as well temperatures allows a change in volume or dimensions. The pressure-dependent calculations of elastic constants will provide a measure of the accuracy of the calculation of forces in SiC as well the mechanical stiffening or hardening attributed to Si–Si,

C–C, and Si–C bond compression and bond strengthening due to lattice vibration.

We express the molecular force in the absence of the Lorentz effective field [19–26].

$$f = \frac{1}{3}\left[\frac{\mathrm{d}^2}{\mathrm{d}r^2}U_{SR}(r) - \frac{2}{r_0}\frac{\mathrm{d}}{\mathrm{d}r}U_{SR}(r)\right]_{r=r_0}, \tag{40}$$

The force constant is a function of the second-order derivatives of the short-range (SR) overlap repulsive potential and as well the charge dipole–dipole and charge dipole–quadruple van der Waals potential. The Reststrahlen frequency is obtained from the force constant using

$$\upsilon_0 = \frac{1}{2\pi}\left[\frac{f}{\mu}\right]^{1/2}, \tag{41}$$

Here, μ is the reduced mass of SiC.

The Grüneisen parameter γ_G is a ratio of second and first-order derivatives of the potentials enable us to discuss the anharmonic effects in a crystal. We express γ_G as

$$\gamma_G = -\frac{r_0}{6}\left[\frac{U'''(r_0)}{U''(r_0)}\right] \tag{42}$$

The pressure dependence of Grüneisen parameter is sketched in Fig. 12a for 3C SiC in ZnS (B3) and RS (B1) phases. A linear decrease of γ_G with pressure in both phases is observed. The Grüneisen constant jump [γ_G (B3 − B1)] at P_T is about 7 % in 3C SiC ceramics. Deduced γ_G value of about 1.015 for 3C SiC in ZnS (B3) phase is in good agreement with available theoretical results [5, 11, 61]. On the other hand, Fig. 12b discerns temperature dependence of Grüneisen parameter with a value of about 0.98 at 1000 K. For most of the solids, Grüneisen parameter ranges from 1.5 to 2.5. As Grüneisen constant γ_G behaviour is influenced by ratio of second and first-order derivatives of the potentials, we may thus comment that anharmonicity is significant in SiC ceramics. Note that these results are further validated by inelastic neutron scattering measurements to probe phonon frequencies as a function of the crystal volume.

The isothermal compressibility (β) is known from second-order derivative of the potential as

$$\beta = \left[\frac{r_0^2}{9V}\{U''(r_0)\}\right]^{-1} \tag{43}$$

The isothermal compressibility (β) is another interesting thermodynamical property which invokes the bond compression or strengthening on application of pressure. With this motivation, we have computed and sketched isothermal compressibility (β) with pressure in Fig. 13a. For SiC, at zero pressure, β is about 0.024 which is comparable with available theoretical result of 0.1518 [5, 11]. Note that the

lattice of SiC is stiffened with increased pressure in *B*3 phase. At phase transition pressure it gets softened. Away from phase transition pressure and at higher pressures i.e., in *B*1 phase *β* again becomes stiff. The mechanical stiffening is reflected from all elastic response of SiC. It is attributed to Si–Si, C–C, and Si–C bond compression and bond strengthening due to lattice vibration in both *B*3 and *B*1 phase. We comment that the compressibility (*β*) at zero pressure is reduced by about 1 % of that at transition pressure P_T in *B*3 phase in SiC. However, the magnitude of *β* at transition pressure P_T is about 0.3 % of that at higher pressures (∼150 GPa). We identify that SiC documents giant lattice softening at the boundary of *B*3–*B*1 phase transition.

The compressibility is useful in engineering applications as it measures the performance of a material explicitly the elasticity, extensibility, and thermal conduction. The isothermal compressibility (*β*) as functions of temperature is shown in Fig. 13b. It is seen that *β* displays a steep increase in *B*3 phase. The compressibility is thus tunable with applied pressure and temperature stimuli and plays a vital role in tailoring materials and composites.

We further compute Debye temperature (θ_D) to shed further light on mechanical stiffened and thermal softened characteristics of SiC following [80–84]:

$$\theta_D^3 = \frac{3.15}{8\pi}\left(\frac{h}{k_B}\right)^3\left(\frac{r}{M}\right)^{\frac{3}{2}}\left(\frac{C_{11}-C_{12}}{2}\right)^{\frac{1}{2}}\left(\frac{C_{11}+C_{12}+2C_{44}}{2}\right)^{\frac{1}{2}}C_{44}^{\frac{1}{2}},$$

(44)

where, *M* is the acoustic mass of SiC. The notations *h* and k_B are the Planck and Boltzmann constants.

The Debye temperature as functions of pressure is plotted in Fig. 14a for SiC. At zero pressure, θ_D is about 611 K. It is noticed that with enhanced pressure, θ_D decreases in *B*3 phase for SiC. The Debye temperature from *B*3 to *B*1 phase is jumped by 655 K at P_T. On the other hand, θ_D showed an increase in *B*1 phase. Deduced value of θ_D is listed in Table 5. Suppressed θ_D in *B*1 phase at higher pressure indicates the mechanical stiffening of lattice and giant softening at P_T and above pressures.

Debye temperature is a function of temperature and its value varies from technique to technique as well as depends on the sample quality. Usually, a standard deviation in θ_D of about 15 K is agreeable. The change in the

Fig. 12 Varaition of Gruneisen parameter (*γ*$_G$) with pressure and temperature
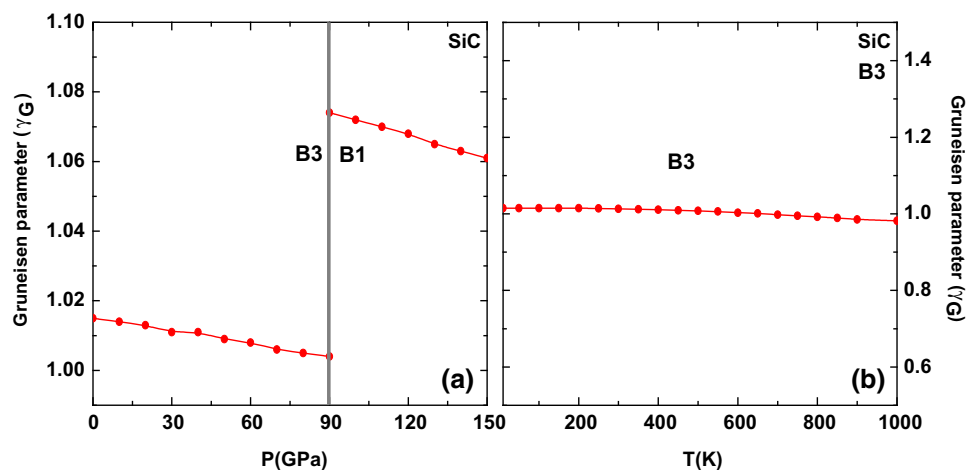
Fig. 13 Variation of isothermal compressibility (*β*) with pressure and temperature
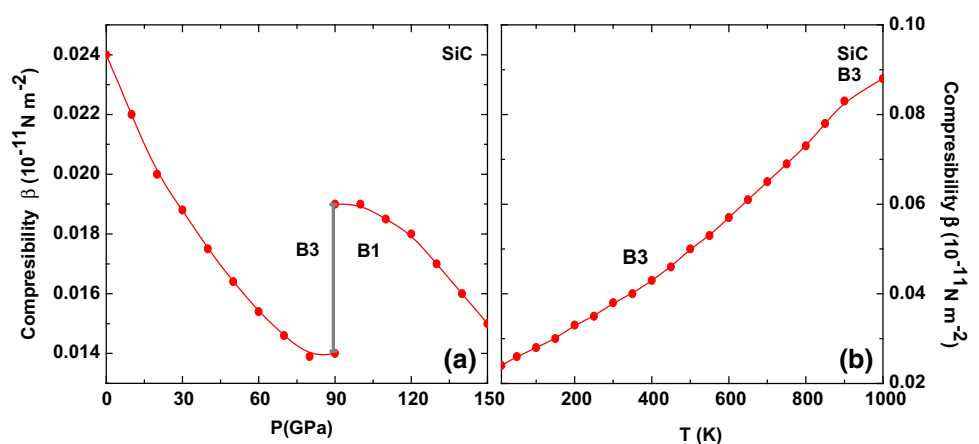
Fig. 14 Variation of Debye temperature (θ_D) as a function of pressure and temperature
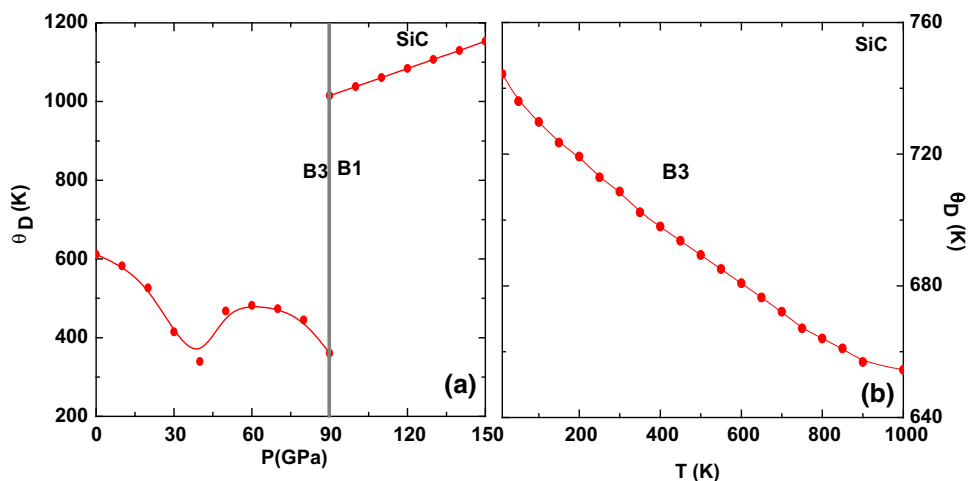
force constants induced by pressure decreases θ_D in $B3$ phase and after transition pressure it starts increasing which drives the system effectively towards the softening of lattice with increasing pressure.

Figure 14b displays the variation of the Debye temperature as functions of temperature at zero pressure. Starting from zero temperature, θ_D decreases rapidly. On the other hand, θ_D enhances with applied pressures at zero temperature. It is worth commenting from high pressure and high temperature Debye temperature behaviour that (a) the pressure-dependent Debye temperature infers the mechanical stiffened bulk modulus due to Si–Si, C–C, and Si–C bond compression and bond strengthening due to lattice vibration and (b) the thermal softening of bulk modulus results from bond expansion and bond weakening due to thermal stress in 3C SiC ceramics in ZB structure.

A comparison of values of $\theta_D(P)$ and $\theta_D(T)$ at zero pressure and zero temperature results: $\theta_D(T) > \theta_D(P)$ implying the susceptibility of θ_D with temperature. It is worth to comment that $\theta_D(P)$ and $\theta_D(T)$ behave differently with applied pressure and temperatures in 3C SiC ceramics. This is attributed to the fact vibrational spectrum of SiC lattice is controlled by aggregate elastic constants C_{ij} behaviour. Thus, the understanding of Debye temperature behaviour of a material not only provides essential features of the vibrational spectrum but is also mandatory for technological and engineering applications. This quantity is useful as a reference for future experimental studies.

The cumulative effect of both pressure and temperature led us to define aggregate elastic constants C_{av} as

$$C_{av.} = \left(\frac{8\pi}{3.15}\right)^{\frac{2}{3}}\left(\frac{k_B}{h}\right)^2\left(\frac{M}{r}\right)\theta_D^2, \tag{45}$$

This is useful once Debye temperature at zero pressure is known from experiments. Despite various investigations on mechanical and thermodynamical properties, basic

properties controlled by elastic constants related with high temperature behaviours are lacking.

In order to further explore the role of anharmonic effects in terms of heat capacity at constant volume C_v and thermal expansion coefficient α, we express the vibration term $A_{vib.}$ [85, 86]:

$$A_{vib.}(\theta_D, T) = nk_BT\left[\frac{9\theta_D}{8T} + 3\ln\left\{1 - \exp\left(-\frac{\theta_D}{T}\right)\right\} - D(\theta_D/T)\right] \tag{46}$$

The non-equilibrium Gibbs function, $G^*(V; P, T)$, is minimized with respect to volume V as

$$\left[\frac{\partial G^*(V; P, T)}{\partial V}\right]_{P,T} = 0 \tag{47}$$

From Eq. (47), we determine heat capacity at constant volume C_v as

$$C_v = 3nk_B\left[4D\left(\frac{\theta_D}{T}\right) - \frac{3\theta_D/T}{e^{\theta_D/T} - 1}\right] \tag{48}$$

Figure 15a documents the variations of heat capacity at constant volume, C_v, with pressure P for both $B3$ and $B1$ phase of SiC at $T = 600$, 800, 1000 and 1200 K. The normalized heat capacity is $[C_v(P) - C_v(0)]/C_v(0)$, where $C_v(P)$ and $C_v(0)$ are heat capacity at any pressure P and at zero pressure. Starting from zero pressure, normalized heat capacity initially increases and with further enhanced pressure it decreases abruptly in $B1$ phase. This behaviour essentially points to the fact that the SiC lattice vibrations energy are controlled by both pressure as well temperature. Note that for higher temperatures $T \rightarrow \theta_D$, the variation in heat capacity with pressure is weak in $B1$ phase. Also, at P_T, reduced jump in between ZB and RS structures can be seen as compared to low temperatures.

The Debye temperature calculated from elastic constants must have a close resemblance to that measured from

Fig. 15 Variation of heat capacity (C_v) with pressure at different temperatures and with temperature at different pressures
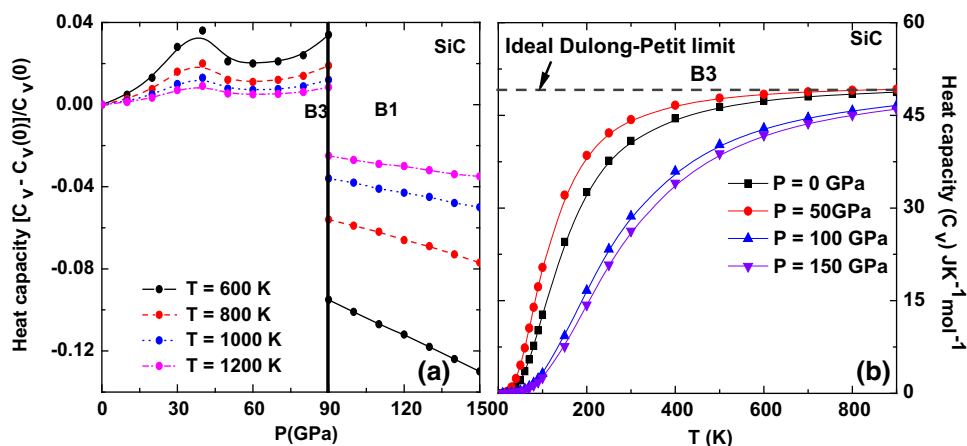
specific heat only at low temperatures. It is instructive to study the temperature-dependent behaviour of heat capacity. Figure 15b illustrates the heat capacity at constant volume, C_v, behaviour as functions of temperature for various pressures [0, 50, 100, 150 GPa] within the framework of quasi-harmonic model for 3C SiC ceramics. It can be seen that below room temperature (300 K), C_v increases very rapidly with the temperature at all pressures. Above room temperature, C_v increases slowly with the temperature. It almost approaches a constant ideal gas limit, the Dulong–Petit limit, $C_v(T) = 3R$, at higher temperatures as well at all pressures for SiC ceramics.

We further determine thermal expansion coefficient $\alpha_{th.exp.}$ using Eq. (47) as

$$\alpha_{th.exp.} = \frac{\gamma C_v}{B_T V} \qquad (49)$$

Apart from the pressure dependence of heat capacity at constant volume C_v, the Gruneisen parameter and Bulk modulus are also needed to elucidate the thermal expansion coefficient ($\alpha_{th.exp.}$). It is a measure of any alteration in phonon frequency depending on the lattice's expansion or contraction in volume as a result of temperature variation. Figure 16a illustrates the pressure dependence of $\alpha_{th.exp.}$ for 3C SiC in both ZB and RS i.e., B3 and B1 phase. A non-linear decrease in $\alpha_{th.exp.}$, is thus witnessed with pressure in both ZnS and NaCl phase. The decrease is more rapid in ZB structure while a slow decrease is documented in RS structure. We note that at P_T, the thermal expansion coefficient $\alpha_{th.exp.}$ is suppressed by 26–22 % in SiC, at temperatures 600, 800, 1000, and 1200 K, respectively.

The variations of $\alpha_{th.exp.}$ as functions of temperature at various pressures have been plotted in Fig. 16b for 3C SiC ceramics. This figure shows that at low temperatures ($T < 250$ K), $\alpha_{th.exp.}$ enhances rapidly with temperature at $P = 0$ and 50 GPa. At high temperatures ($T > 250$ K), a sharp increase of $\alpha_{th.exp}$ is witnessed at all pressures. This

figure also suggests that with enhanced pressure, the increase of $\alpha_{th.exp.}$ with temperature becomes smaller. In other words, the slope of $\alpha_{th.exp.}$ gradually decreases at higher temperatures at all pressures except at $P = 0$ GPa. Returning back to pressure dependence of thermal expansion coefficient ($\alpha_{th.exp.}$), we note a rapid decrease in ZB structure with the increase of pressure. A comparison of $\alpha_{th.exp.}(P)$ and $\alpha_{th.exp.}(T)$ reveals that $\alpha_{th.exp.}(P)$ values are smaller than that $\alpha_{th.exp.}(T)$ for SiC under same pressure and temperature. Thus, $\alpha_{th.exp.}(P)$ and $\alpha_{th.exp.}(T)$ are differently sensitive to the Si and C ions in 3C SiC ceramics as SiC lattice is mechanical hard due to bond strengthening and thermal soft due to bond weakening.

Concluding remarks

The present study addresses for the first time, the high pressure and high temperature-dependent structural, elastic, and thermodynamical studies in ZB and RS structure of 3C SiC ceramics. We have formulated an interatomic pairwise potential that incorporates the long-range Coulomb with charge transfer interactions, covalent nature of bonds, zero point energy effects and the short-range interactions as charge dipole–dipole and charge dipole–quadruple (van der Waals), as well overlap repulsive interaction up to second-neighbour ions.

From the knowledge of Gibbs's free energies in ZB and RS structure, we determine the pressure-induced first-order structural phase transition of SiC at about 90 GPa. As a next step, we determine the cohesive energy as 6.301 eV for 3C SiC ceramics and the volume collapse is about 13.8 %. Compressions in SiC at higher pressure indicate the mechanical stiffening of lattice. The phase transition pressure and volume collapse are consistent with earlier observations. We emphasize that agreement with experimental and theoretical data is not fortuitous, but it is

Fig. 16 Variation of the thermal expansion coefficient ($\alpha_{\text{th.exp.}}$) with pressure at different temperatures and with temperature at different pressures
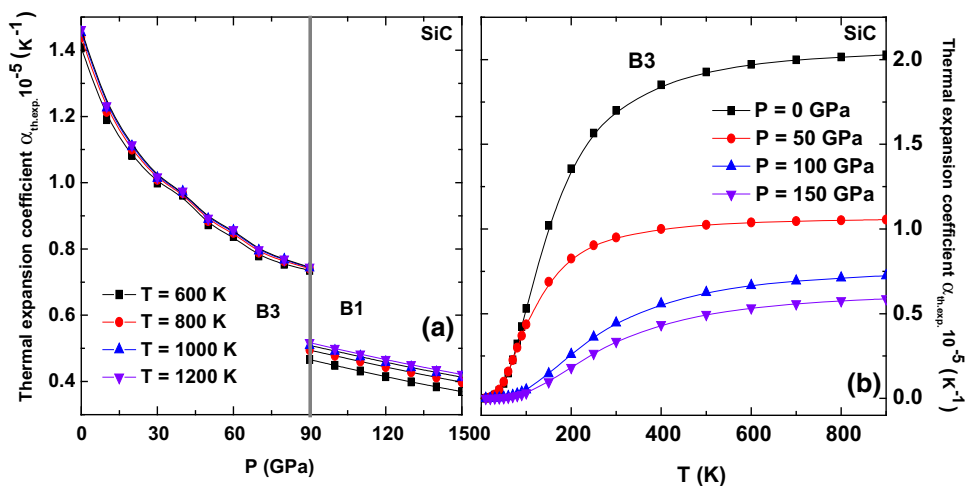
attributed to proper parametrization and formulation of potential with non-central many body forces in terms of the screening of the effective Coulomb potential through modified ionic charge.

Furthermore, we make effort to determine the second-order aggregate elastic constants C_{ij} under applied pressure and temperature with respect to finite strain. Once pressure and temperature dependence of C_{ij} is known, Cauchy discrepancy and elastic anisotropy in second-order elastic constants, melting temperature, third-order elastic constants C_{ijk}, Cauchy discrepancy and anisotropy in third-order elastic constants, isotropic shear moduli as G_H, G_V, and G_R, Young's modulus E, Poisson's ratio ν, Pugh's ratio ϕ and Vicker's hardness H_V to discuss ductile/brittle nature and mechanical stiffening/thermal softening of SiC lattice. In continuity, Lamé's constant (λ, μ), longitudinal (shear) wave velocity to enumerate the compressibility and shear stiffness of the material, Grüneisen constant, Debye temperature, isothermal compressibility, heat capacity and thermal expansion coefficient to shed light on anharmonicity of $3C$ SiC ceramics. We comment that incorporation of charge transfer interactions, covalent contribution and quantum effects leads to nonzero value of Cauchy discrepancy ($C_{12} - C_{44} \neq 0$) and is a corner stone of the proposed interatomic potential.

From the present investigations on $3C$ SiC ceramics, we draw the following conclusions:

(a) The volume collapse (V_P/V_0) in terms of compressions in SiC at higher pressure indicates the mechanical stiffening of lattice. The expansion of SiC lattice is inferred from steep increase in V_T/V_0 and is attributed to thermal softening of SiC lattice.

(b) Larger deviation in Cauchy discrepancy Δ_1^2 emphasizes the importance of the many body non-central (charge transfer and covalency) interaction and substantial anharmonic effects at high pressures.

(c) Elastic anisotropic parameter γ_1^2 in cubic SiC is negative and largely uninfluenced by application of pressure.

(d) Melting temperature (T_M), Vicker's hardness (H_V), shear modulus (G_H), Young's modulus (E) and bulk modulus (B_T) increase with enhanced pressure showing the hardening or stiffening of the lattice, and suppressed T_M, G_H, E and B_T variations in temperature suggest the weakening of the lattice as a result of thermal softening of SiC lattice.

(e) From the Pugh's ratio (ϕ) we classify $3C$ SiC as ductile material while to that Poisson's ratio suggest its brittle nature. The two empirical rules only differ on the exact border between the two types of behaviour and SiC is a borderline case between the classes of ductile and brittle materials.

(f) Grüneisen parameter (γ_G) Debye temperature (θ_D), isothermal compressibility (β), heat capacity at constant volume (C_v) and thermal expansion coefficient ($\alpha_{\text{th.exp.}}$) probe the importance of anharmonicity in SiC at heigh pressures and temperatures.

(g) Elastic properties showed $T_M(P) < T_M(T)$, $H_V(P) < H_V(T)$, $E(P) < E(T)$, $E(P) < E(T)$, $\theta_D(P) < \theta_D(T)$ and $\alpha_{\text{th.exp.}}(P) < \alpha_{\text{th.exp.}}(T)$ infers that these are differently sensitive to the Si and C ions as SiC lattice is mechanical hard due to bond strengthening and thermal soft due to bond weakening.

To an end, an interatomic pairwise potential for cubic SiC incorporating the non-central many body forces as long-range Coulomb with charge transfer interactions, covalent nature of bonds (due to Si–Si, Si–C, and C–C interacting electric fields), quantum effects, charge

dipole–dipole and charge dipole–quadruple (van der Waals), and the short-range interactions as overlap repulsion up to second-neighbour ions successfully explains the pressure and temperature induced structural, elastic and thermodynamical properties of $3C$ SiC ceramics consistent with available results.

Appendix 1

The relevant expressions for the aggregate second-order elastic constants (SOECs), and the pressure derivatives of SOECs are expressed for zinc-blende structure as

$$C_{11} = L\left[0.2477Z(Z + 8f(r_0)) + \frac{1}{3}(A_1 + 2B_1)\right.$$
$$\left. + \frac{1}{2}(A_2 + B_2) + 5.8243Zaf'(r_0)\right], \quad (50)$$

$$C_{12} = L\left[-2.6458Z(Z + 8f(r_0)) + \frac{1}{3}(A_1 - 4B_1)\right.$$
$$\left. + \frac{1}{4}(A_2 - 5B_2) + 5.8243Zaf'(r_0)\right], \quad (51)$$

$$C_{44} = L\left[-0.123Z(Z + 8f(r_0)) + \frac{1}{3}(A_1 + 2B_1) + \frac{1}{4}(A_2 + 3B_2)\right.$$
$$\left. - \frac{1}{3}\nabla(-7.53912Z(Z + 8f(r_0)) + A_1 - B_1)\right] \quad (52)$$

and

$$B_1 + B_2 = -1.261Z[Z + 8f(r)]. \quad (53)$$

Thus, second-order elastic constants difference lead to finite value at Cauchy pressure:

$$C_{12} - C_{44} \neq 0 \quad (54)$$

Henceforth, polarizability of the ions has effect on the elastic constants. It should be noted that if charge transfer mechanism is not taken into account, Cauchy relation: $C_{12} - C_{44} = 0$, The Cauchy violations ($C_{12} \neq C_{44}$) is seen by several crystals due to anisotropy in the electron distribution or angle bending. Here, C_{11} represents a measure of resistance to deformation by applied stress and C_{44} represents the measure of resistance to deformation with respect to applied shearing stress. The elastic constants C_{12} and C_{44} are related to the elasticity in shape, which is a shear constant.

The pressure derivatives of second-order elastic constants under hydrostatic pressure P are obtained in the form

$$3\Omega \frac{dB_T}{dp} = -\left[20.1788Z(Z + 8f(r_0)) - 3(A_1 + A_2)\right.$$
$$+ 4(B_1 + B_2) + 3(C_1 + C_2) - 104.8433Zaf'(r_0)$$
$$\left. + 22.7008Za^2f''(r_0)\right] \quad (55)$$

$$2\Omega \frac{d\sigma}{dp} = -\left[-11.5756Z(Z + 8f(r_0)) + 2(A_1 - 2B_1)\right.$$
$$\left. + \frac{3}{2}A_2 - \frac{7}{2}B_2 + \frac{1}{4}C_2 + 37.5220Zaf'(r_0)\right], \quad (56)$$

and

$$\Omega \frac{dC_{44}}{dp} = -\left[\begin{array}{l} 0.4952Z(Z + 8f(r_0)) + \frac{1}{3}(A_1 - 4B_1 + C_1)r \\ + \frac{1}{4}(2A_2 - 6B_2 + C_2) + 4.9667Zaf'(r_0) + 2.522Za^2f''(r_0) \end{array}\right]$$
$$+ \nabla\left[-17.5913Z(Z + 8f(r_0)) + A_1 - B_2 - \frac{2}{3}C_{11}\right.$$
$$\left. + 40.6461Zaf'(r_0) - 5.044Za^2f''(r_0)\right]$$
$$+ \nabla^2\left[3.1416Z(Z + 8f(r_0) + \frac{2}{3}(A_1 - B_1)\right.$$
$$\left. + \frac{C_1}{3} - 15.9412Zaf'(r_0) + 8.8052Za^2f''(r_0)\right] \quad (57)$$

The notations are

$$\Omega = -5.0440g + A_1 + A_2 - 2(B_1 + B_2) + 17.4730Zg_1 \quad (58)$$

$$\nabla = \left[\frac{-7.5391Z(Z + 8f(r_0)) + (A_1 - B_1)}{-3.141Z(Z + 8f(r_0)) + (A_1 + 2B_1) + 21.765Zaf'(r_0)}\right], \quad (59)$$

Finally, the anharmonic third-order elastic constants (TOECs) for zinc-blende structure are as follows:

$$C_{111} = \frac{e^2}{4a^4}\left[0.5184g + \frac{1}{9}(C_1 - 6B_1 - 3A_1) + \frac{1}{4}(C_2 - B_2 - 3A_2)\right.$$
$$\left. - 2(B_1 + B_1) - 9.9326Zg_1 + 2.522Zg_2\right], \quad (60)$$

$$C_{112} = \frac{e^2}{4a^4}\left[0.3828g + \frac{1}{9}(C_1 + 3B_1 - 3A_1) + \frac{1}{8}(C_2 + 3B_2 - 3A_2)\right],$$
$$- 11.642Zg_1 + 2.522Zg_2 \quad (61)$$

$$C_{123} = \frac{e^2}{4a^4}\left[6.1585g + \frac{1}{9}(C_1 + 3B_1 - 3A_1) - 12.5060Zg_1 + 2.5220Zg_2\right], \quad (62)$$

$$C_{144} = \frac{e^2}{4a^4}\left\{6.1585g + \frac{1}{9}(C_1 + 3B_1 - 3A_1) - 4.1681Zg_1 + .8407zg_2 + \right.$$
$$+ \nabla\left[-3.3507g - \frac{2}{9}C_1 + 13.5486Zg_1 - 1.681Zg_2\right]$$
$$\left. + \nabla^2\left[-1.5637g + \frac{2}{3}(A_1 - B_1) + \frac{C_1}{9} - 5.3138Zg_1 + 2.9350Zg_2\right]\right\} \quad (63)$$

$$C_{166} = \frac{e^2}{4a^4}\Bigg\{ -2.1392g + \frac{1}{9}(C_1 - 6B_1 - 3A_1) + \frac{1}{8}(C_2 - 5B_2 - 3A_2) - (B_1 - B_2)$$

$$-4.168Zg_1 + .8407Zg_2 + \nabla\Big[-8.3768g + \frac{2}{3}(A_1 - A_2) - \frac{2}{9}C_1 + 13.5486Zg_1 - 1.6813Zg_2\Big] \tag{64}$$

$$+\nabla^2\Big[2.3527g + \frac{C_1}{9} - 5.3138Zg_1 + 2.9350Zg_2\Big]$$

$$C_{456} = \frac{e^2}{4a^4}\Bigg\{4.897g + \frac{1}{9}(C_1 - 6B_1 - 3A_1) - B_2 + \nabla\Big[-5.0261g - \frac{1}{9}C_1\Big]$$

$$+\nabla^2\Big[7.0580g + \frac{1}{3}C_1\Big] + \nabla^3\Big[-4.8008g + \frac{1}{3}(A_1 - B_1) - \frac{1}{9}C_1\Big]\Bigg\} \tag{65}$$

In view of equilibrium condition, the third-order elastic constants difference also lead to finite value at Cauchy pressure inferring that polarizability of the ions has effect on the elastic constants:

$$C_{112} - C_{166} \neq 0 \tag{66}$$

$$C_{123} - C_{456} \neq 0 \tag{67}$$

$$C_{144} - C_{456} \neq 0 \tag{68}$$

$$C_{123} - C_{144} \neq 0 \tag{69}$$

Furthermore, the third-order elastic constants satisfy the identity:

$$C_{123} + 2C_{456} - 3C_{144} = 0 \tag{70}$$

Various symbols appear in the earlier expressions are associated with the crystal energy and have been defined below:

$$A_1 = A_{ij} = \frac{4a^3}{e^2}\left(\frac{\mathrm{d}^2}{\mathrm{d}r^2}V_{ij}(r)\right)_{r=a}, \tag{71}$$

$$A_2 = A_{ii} = A_{jj} = \frac{4a^3}{e^2}\left(\frac{\mathrm{d}^2}{\mathrm{d}r^2}V_{ii}(r) + \frac{\mathrm{d}^2}{\mathrm{d}r^2}V_{jj}(r)\right)_{r=\sqrt{3}a/4}, \tag{72}$$

$$B_1 = B_{ij} = \frac{4a^2}{e^2}\left(\frac{\mathrm{d}}{\mathrm{d}r}V_{ij}(r)\right)_{r=a}, \tag{73}$$

$$B_2 = B_{ii} = B_{jj} = \frac{4a^2}{e^2}\left(\frac{\mathrm{d}}{\mathrm{d}r}V_{ii}(r) + \frac{\mathrm{d}}{\mathrm{d}r}V_{jj}(r)\right)_{r=\sqrt{3}a/4}, \tag{74}$$

$$C_1 = C_{ij} = \frac{4a^4}{e^2}\left(\frac{\mathrm{d}^3}{\mathrm{d}r^3}V_{ij}(r)\right)_{r=a}, \tag{75}$$

$$C_2 = C_{ii} = C_{jj} = \frac{4a^4}{e^2}\left(\frac{\mathrm{d}^3}{\mathrm{d}r^3}V_{ii}(r) + \frac{\mathrm{d}^3}{\mathrm{d}r^3}V_{jj}(r)\right)_{r=a}, \tag{76}$$

$$g = Z + 8f(r) \tag{77}$$

$$g_1 = r_o \mathrm{d}f(r) \tag{78}$$

$$g(2) = r_o d\mathrm{d}f(r) \tag{79}$$

Similarly, the expressions for the second-order elastic constants for RS structure crystals are as follows:

$$C_{11} = \frac{e^2}{4a^4}\left\{-5.112Z_m^2 + A_1 + \frac{A_2 + B_2}{2} + 9.3204Z(af'(r))\right\} \tag{80}$$

$$C_{12} = \frac{e^2}{4a^4}\left\{0.226Z_m^2 - B_1 + \frac{A_2 - 5B_2}{4} + 9.3204Z(af'(r))\right\} \tag{81}$$

$$C_{44} = \frac{e^2}{4a^4}\left\{2.556Z_m^2 + B_1 + \frac{A_2 + 3B_2}{4}\right\} \tag{82}$$

and

$$B_1 + B_2 = -1.165Z[Z + 12f(r)]. \tag{83}$$

For non-central many body forces as we deal with the second-order elastic constants difference lead to finite value at Cauchy pressure:

$$C_{12} - C_{44} \neq 0 \tag{84}$$

The pressure derivatives of second-order aggregate elastic constants under hydrostatic pressure P are obtained in the form

$$3\Omega\frac{\mathrm{d}B_T}{\mathrm{d}p} = -\big\{13.980Z_m^2 + C_1 - 3A_1 + C_2 - 3A_2$$

$$-167.7648Z(af'(r)) + 41.9420Z(a^2f''(r))\big\} \tag{85}$$

$$2\Omega\frac{\mathrm{d}\sigma}{\mathrm{d}p} = -\Big\{23.682Z_m^2 + C_1 + \frac{C_2 + 6A_2 - 6B_2}{4}$$

$$-50.0752Z(af'(r)) + 13.9808Z(a^2f''(r))\Big\} \tag{86}$$

$$\Omega \frac{\mathrm{d}C_{44}}{\mathrm{d}p} = -\Big\{ -11.389Z_m^2 + A_1 - 3B_1$$
$$+ \frac{C_2 + 2A_2 - 10B_2}{4} + 44.6528Z(af'(r)) \Big\} \tag{87}$$

The notation Ω is

$$\Omega = -2.330Z_m^2 + A_1 + A_2 + 27.9612Z(af'(r)) \tag{88}$$

Finally, the anharmonic third-order elastic constants for RS structure are as follows:

$$C_{111} = \frac{e^2}{4a^4} \Big\{ 37.556Z_m^2 + C_1 - 3A_1 - \frac{3A_2 + 9B_2 - C_2}{4}$$
$$-89.305Z(af'(r)) + 13.980Z(a^2f''(r)) \Big\} \tag{89}$$

$$C_{112} = \frac{e^2}{4a^4} \Big\{ -4.836Z_m^2 - \frac{3A_2 + 3B_2 - C_2}{8}$$
$$-18.640Z(af'(r)) + 4.66Z(a^2f''(r)) \Big\} \tag{90}$$

$$C_{123} = \frac{e^2}{4a^4} \Big\{ 2.717Z_m^2 + 16.692Z(af'(r)) \Big\} \tag{91}$$

$$C_{144} = \frac{e^2}{4a^4} \Big\{ 2.717Z_m^2 + 5.564Z(af'(r)) \Big\} \tag{92}$$

$$C_{166} = \frac{e^2}{4a^4} \Big\{ -4.836Z_m^2 - 2(B_1 + B_2)$$
$$- \frac{3A_2 - 3B_2 - C_2}{8} + 5.564Z(af'(r)) \Big\} \tag{93}$$

$$C_{456} = \frac{e^2}{4a^4} \Big\{ 2.717Z_m^2 - (B_1 + B_2) \Big\} \tag{94}$$

Various symbols appear in the above expressions are associated with the crystal energy and have the following form in RS structure

$$A_1 = \frac{8a^3}{e^2} \left[\frac{\mathrm{d}^2}{\mathrm{d}r^2} V_{ij}(r) \right]_{r=a}, \tag{95}$$

$$A_2 = \frac{16a^3}{e^2} \left[\frac{\mathrm{d}^2}{\mathrm{d}r^2} V_{ii}(r) + \frac{\mathrm{d}^2}{\mathrm{d}r^2} V_{jj}(r) \right]_{r=\sqrt{2}a}, \tag{96}$$

$$B_1 = \frac{8a^3}{e^2} \left[\frac{1}{r} \frac{\mathrm{d}}{\mathrm{d}r} V_{ij}(r) \right]_{r=a}, \tag{97}$$

$$B_2 = \frac{16a^3}{e^2} \left[\frac{1}{r} \frac{\mathrm{d}}{\mathrm{d}r} V_{ii}(r) + \frac{1}{r} \frac{\mathrm{d}}{\mathrm{d}r} V_{jj}(r) \right]_{r=\sqrt{2}a}, \tag{98}$$

$$C_1 = \frac{8a^3}{e^2} \left[r \frac{\mathrm{d}^3}{\mathrm{d}r^3} V_{ij}(r) \right]_{r=a}, \tag{99}$$

$$C_2 = \frac{16a^3}{e^2} \left[r \frac{\mathrm{d}^3}{\mathrm{d}r^3} V_{ii}(r) + \frac{\mathrm{d}^3}{\mathrm{d}r^3} V_{jj}(r) \right]_{r=\sqrt{2}a} \tag{100}$$

in terms of the short-range energy

$$V_{ij}(r) = \sum_{ij} b\beta_{ij} \exp\left(\frac{r_i + r_j - r_{ij}}{\rho} \right) - \sum_{ij} \frac{C}{r_{ij}^6} - \sum_{ij} \frac{D}{r_{ij}^8} \tag{101}$$

The short-range interaction (SR) energy is expressed in terms of the overlap repulsion (first term) and the induced charge dipole–dipole and charge dipole–quadruple (van der Waals) [second and third terms], respectively.

Appendix 2

The temperature-dependent elastic, thermal and thermodynamical properties of SiC are now studied within the quasi-harmonic Debye approximation. The Helmholtz free energy at temperature below the melting point of SiC ceramics in the quasi-harmonic model is applicable to evaluate equation of state and thus the elastic properties. The non-equilibrium Gibbs's free energy function, $G^*(V; P, T)$ within the quasi-harmonic approximation is $G = U + PV + A_{\mathrm{vib.}}[\theta_D(V); T]$.

In order to determine the anharmonic effects on the elastic constants at higher temperatures, we use the equation of state (EOS) as:

$$P = -\frac{\mathrm{d}U}{\mathrm{d}V} + T\alpha_v B_T \tag{102}$$

Here, P is the pressure, T the temperature, U the total potential energy, α_v the volume thermal expansion coefficient, B_T the isothermal bulk modulus. The second term in Eq. (106) is the thermal phonon pressure. The temperature-dependent second-order elastic constants C_{ij} are derived from the dynamical matrix of modified Rigid Shell model [19–26, 35–42] and the method of long waves as

$$C_{11} = 1.573T\alpha_v B_T$$
$$+ \frac{e^2}{4a^4} \Big\{ \frac{1}{3}A_1 - 0.9B_1 - 1.573B_2 + 8.9558(af'(r)) \Big\} \tag{103}$$

$$C_{12} = -1.786T\alpha_v B_T$$
$$+ \frac{e^2}{4a^4} \Big\{ \frac{1}{3}A_1 + 1.45B_1 + 1.786B_2 + 8.9558(af'(r)) \Big\} \tag{104}$$

$$C_{44} = -0.786T\alpha_v B_T$$
$$+ \frac{e^2}{4a^4} \Big\{ \frac{1}{3}A_1 + 1.45B_1 + 1.786B_2 - \frac{1}{3}\Delta \Big\} \tag{105}$$

with

$$\Delta = \left[A_1 + 6.77B_1 + 7.78B_2 - 7.77 \left\{ T\alpha_v B_T \frac{4a^4}{e^2} \right\} \{ (A_1 + 2B_1) + 3(A_2 + 2B_2) \}^{-1} \right]$$

(106)

and

$$T\alpha_v B_T = \frac{e^2}{4a^4} [1.9395Z[Z + 8f(r_0)] + (B_1 + B_2)] \qquad (107)$$

Herein, the potential energy incorporates the long-range Coulomb with charge transfer interactions, covalent nature of bonds, and short-range overlap repulsive interaction up to second-neighbour as well charge dipole–dipole and charge dipole–quadruple (van der Waals) interaction.

We use equilibrium condition to obtain temperature dependence of hardness and range parameters as

$$r \left| \frac{dU(r)}{dr} \right|_{r=r_0} = 3T\alpha_v V B_T \qquad (108)$$

Here, V is the unit cell volume of SiC.

References

1. Levinshtexin, M.E., Rumyantsev, S.L., Shur, M.: Properties of advanced semiconductor materials: GaN, AlN, InN, BN, SiC, SiGe. Wiley, New York (2001)
2. Parfenova, I.I.: Substitutional 3d impurities in cubic silicon carbide. Semiconductors **38**, 189 (2004)
3. Yoshida, M., Onodera, A., Ueno Takemura, M.K., Shimomura, O.: Pressure-induced phase transition in SiC. Phys. Rev. B **48**, 10587 (1993)
4. Sekine, T., Kobayashi, T.: Shock compression of 6*H* polytype SiC to 160 GPa. Phys. Rev. B **55**, 803 (1997)
5. Chang, K.J., Cohen, M.L.: Ab initio pseudopotential study of structural and high-pressure properties of SiC. Phys. Rev. B **35**, 8196 (1987)
6. Miao, M.S., Lambrecht, W.R.L.: Unified path for high-pressure transitions of SiC polytypes to the rocksalt structure. Phys. Rev. B **68**, 92103 (2003)
7. Durandurdu, M., Drabold, D.A.: *Ab initio* simulations of the structural phase transformation of 2*H*-SiC at high pressure. Phys. Rev. B **75**, 235204 (2007)
8. Shimojo, F., Ebbsj, O.I., Lalia, R., Nakano, A., Rino, J.P., Vashista, P.: Molecular dynamics simulation of structural transformation in silicon carbide under pressure. Phys. Rev. Lett. **84**, 3338 (2000)
9. Yu-Ping, L., Duan-Wei, H., Jun, Z., Xiang Dong, Y.: First-principles study of pressure-induced phase transition in silicon carbide. Phys. B **403**, 3543 (2008)
10. Vashishta, P., Kalia, R.K., Nakano, A.: Interaction potential for silicon carbide: A molecular dynamics study of elastic constants and vibrational density of states for crystalline and amorphous silicon carbide. J. Appl. Phys. **101**, 103515 (2007)
11. Cheong, B.H.K., Chang, J., Cohen, M.L.: Pressure dependences of band gaps and optical-phonon frequency in cubic SiC. Phys. Rev. B **44**, 1053 (1991)
12. Miao, M.S., Prikhodko, M., Lambrecht, W.R.L.: Changes of the geometry and band structure of SiC along the orthorhombic high-pressure transition path between the zinc-blende and rocksalt structures. Phys. Rev. B **66**, 64107 (2002)
13. Miao, M.S., Prikhodko, M., Lambrecht, W.R.L.: Orthorhombic intermediate state in the zinc blende to rocksalt transformation path of SiC at high pressure. Phys. Rev. Lett. **88**, 18960 (2002)
14. Durandurdu, M.: Pressure-induced phase transition of SiC. J. Phys. Condens. Matter **16**, 4411–4417 (2004)
15. Stillinger, F.H., Weber, T.A.: Computer-simulation of local order in condensed phases of silicon. Phys. Rev. B **31**, 5262 (1985)
16. Karch, K., Bechstedt, F., Pavone, P., Strauch, D.: Pressure-dependent properties of SiC polytypes. Phys. Rev. B **53**, 13400 (1996)
17. Oganov, A.R. (ed.): Modern methods of crystal structure prediction (2011) Wiley VCH Verlag GmbH and Co. KGaA, Weinheim
18. Dion, M., Rydberg, H., Schroder, E., Langreth, D.C., Lundqvist, B.I.: Van der Waals density functional for general geometries. Phys. Rev. Lett. **92**, 246401 (2004)
19. Varshney, D., Kaurav, N., Sharma, P., Shah, S., Singh, R.K.: Structural phase transition and elastic properties of ZnSe at high pressure. Phase Transit **77**, 1075 (2004)
20. Varshney, D., Sharma, P., Kaurav, N., Shah, S., Singh, R.K.: Study of elastic properties and their pressure dependence of semi magnetic semiconductors. J. Phys. Soc. **74**, 382 (2005)
21. Varshney, D., Kaurav, N., Kinge, R., Singh, R.K.: B1-B2 structural phase transition and elastic properties of UX (X = S, Se and Te) compounds at high pressure. J. Phys. Condens. Matter **19**, 236204 (2007)
22. Varshney, D., Sharma, U., Kaurav, N.: Structural phase transformation and mechanical properties of semimagnetic semiconductors $Zn_{1-x}M_xSe$ (M = Mn, Fe and Cd). J. Phys. Condens. Matter **20**, 075204 (2008)
23. Varshney, D., Joshi, G., Kaurav, N., Singh, R.K.: Structural phase transition (zincblende–rocksalt) and elastic properties in AlY (Y = N, P and As) compounds: pressure-induced effects. J. Phys. Chem. Solids **70**, 451 (2009)
24. Varshney, D., Joshi, G.: High-pressure structural phase transition and elastic properties of $Ga_{1-x}In_xAs$ semiconducting compounds. Eur. Phys. J. B **70**, 523 (2009)
25. Varshney, D., Joshi, G., Varshney, M., Shriya, S.: Pressure induced structural phase transition and elastic properties in BSb, AlSb, GaSb and InSb compounds. Phys. B **405**, 1663 (2010)
26. Varshney, D., Joshi, G., Varshney, M., Shriya, S.: Pressure dependent elastic and structural (B 3–B1) properties of Ga based monopnictides. J. Alloys Compd. **495**, 23 (2010)
27. Hafemeister, D.W., Flygare, W.H.: Outer-shell overlap integral as a function of distance for halogen–halogen, halogen–alkali, and alkali–alkali ions in the alkali halide lattices. J. Chem. Phys. Soc **43**, 795 (1965)
28. Tosi, M.P.: Cohesion of ionic solids in the born model. Solid State Phys. **16**, 1 (1964)
29. Born, M., Huang, K.: Dynamical Theory of Crystal Lattices. Clarendon, Oxford (1956)
30. Motida, K.: Szigeti charge and its correlation with hyperine coupling constant of doped Mn^{2+} ion in divalent metal compounds. J. Phys. Soc. Jpn. **49**, 213 (1980)
31. Motida, K.: Effect of covalency on phonon dispersion relations in NaCl type alkali halide crystal. J. Phys. Soc. Jpn. **55**, 1636 (1986)
32. Slater, J.C., Kirkwood, J.G.: The vander Waals forces in gases. Phys. Rev. **37**, 682 (1931)
33. Lowdin, P.O.: Quantum theory of cohesive properties of solids. Adv. Phys. **5**, 1 (1956)
34. Lundqvist, S.O.: Three body potential for alkali halides. Ark. Fys. **12**, 263 (1957)
35. Varshney, D., Joshi, G., Varshney, M., Shriya, S.: Pressure induced mechanical properties of boron-based pnictides. Solid State Sci. **12**, 864 (2010)

36. Varshney, D., Dodiya, N., Shaikh, M.W.: Structural properties and electrical resistivity of Na-substituted lanthanum manganites: $La_{1-x}Na_xMnO_{3+y}$ ($x = 0.1$, 0.125 and 0.15). J. Alloys Compd. **509**, 7447 (2011)

37. Varshney, D., Choudhary, D., Shaikh, M.W., Khan, E.: Electrical resistivity behaviour of sodium substituted manganites: electron–phonon, electron–electron and electron–magnon interactions. Eur. Phys. J. B **76**, 327 (2010)

38. Varshney, D., Kaurav, N., Kinge, R., Singh, R.K.: High-pressure induced structural phase transition in alkaline earth CaX (X = S, Se and Te) semiconductors: NaCl-type (*B*1) to CsCl-type (*B*2). J. Alloys Compd. **484**, 239 (2009)

39. Varshney, D., Kaurav, N., Kinge, R., Singh, R.K.: Pressure induced phase transition (B1–B2) and elastic properties in alkaline earth BaX (X = S, Se and Te) chalcogenides. Phase Transit. **81**, 1 (2008)

40. Varshney, D., Kaurav, N., Kinge, R., Singh, R.K.: High pressure structural (B1–B2) phase transition and elastic properties of II–VI semiconducting Sr chalcogens. Comput. Mater. Sci. **41**, 529 (2008)

41. Varshney, D., Kaurav, N., Sharma, U., Singh, R.K.: Pressure induced phase transition and elastic properties of Y and Sc antimonides. J. Alloys Compd. **448**, 250 (2008)

42. Varshney, D., Kaurav, N., Kinge, R., Shah, S., Singh, R.K.: Study of elastic properties and their pressure dependence of lanthanum monochalcogenides. High Press. Res. **25**, 145 (2005)

43. Tessman, J.R., Kahn, A.H., Shockley, W.: Electronic polarizabilities of ion in crystals. Phys. Rev. **92**, 890 (1953)

44. Shannon, R.D.: Dielectric polarizabilities of ions in oxides and fluorides. J. Appl. Phys. **73**, 348 (1993)

45. Weast, R.C. (ed.): Handbook of Chemistry and Physics, 63rd edn. CRC, BocaRaton (1982)

46. Aleksandrov, I.V., Goncharov, A.F., Stishov, S.M., Yakovenko.: Equation of state and Raman scattering in cubic BN and SiC at high pressure. EV, Pis'ma h.Eksp. Teor. Fiz. **50**, 116 (1989) (JETP Lett. **50**, 127 (1989))

47. Feldman, D.W., Parker, H., Choyke, W., Patric, L.: Phonon dispersion curves by Raman scattering in SiC polytypes 3C, 4H, 6H, 15R, and 21 R. Phys. Rev. **173**, 787 (1968)

48. Jun, L., Vohra, Y.K.: Raman modes of 6H polytype of silicon carbide to ultrahigh pressures: a comparison with silicon and diamond. Phys. Rev. Lett **72** 4105 (1994)

49. Wagman, D.D., Evans, W.H., Parker, V.B., Halow, E., Baily, S.M., Shumm, R.H.: Selected values of chemical thermodynamics properties, tables for the first thirty four elements in the standard order of arrangement, Natl. Bur. Std. (U.S.) Tech. Note No. 270-3 (U.S. GPO, Washington, DC, 1968)

50. Lambrecht, W.R.L., Segall, B., Methfessel, M., van Schilfgaarde, M.: Calculated elastic constants and deformation potentials of cubic SiC. Phys. Rev. B **44**, 3685 (1991)

51. Murnaghan, F.D.: The compressibility of media under extreme, pressures. Proc. Natl. Acad. Sci. U. S. A. **3**, 244 (1944)

52. Goel, P., Choudhury, N., Chaplot, S.L.: Superionic behavior of lithium oxide Li_2O: a lattice dynamics and molecular dynamics study. Phys. Rev. B **70**, 174307 (2004)

53. Xiao-Feng, Li, Xiang-Rong, Chen, Chuan-Min, Meng, Guang-Fu, Ji: Ab initio calculations of elastic constants and thermodynamic properties of Li_2O for high temperatures and pressures. Solid State Commun. **139**, 197–200 (2006)

54. Yun-Dong, G., Ze-Jin, Y., Qing-He, G., Zi-Jiang, L., Wei, D.: The phase transition, and elastic and thermodynamic properties of CaS derived from first-principles calculations. J. Phys. Condens. Matter **20**, 115203 (2008)

55. Kunc, K., Balkanski, M.: Nusimovici MA Lattice dynamics of several A *N*B8–*N* compounds having the zincblende structure II. Numerical calculations. Phys. Status Solidi (b) **72**, 229 (1975)

56. Lee, D.H., Joannopoulos, J.D.: Simple scheme for deriving atomic force constants. Application to SiC. Phys. Rev. Lett. **48**, 1846 (1982)

57. Denteneer, P.J.H., van Haeringen, W.: Ground-state properties of polytypes of silicon carbide. Phys. Rev. B **33**, 2831 (1986)

58. Tolpygo, K. B. Optical, elastic and piezoelectric properties of ionic and covalent with the ZnS type lattice. F. Tverd. Tela (Leningrad) 1960; **2**:2655 Sov. Phys. Solid State 1961; **2**:2367

59. Yean Jr, D.H., Riter, J.R.: Estimates of isothermal bulk moduli for group iva crystals with the zinc blende structure. J. Phys. Chem. Solids **32**, 653 (1971)

60. Carnahan, R.D.J.: Elastic properties of silicon carbide. Am. Ceram. Soc. **51**, 223 (1968)

61. Churcher, N., Kunc, K., Heine, V.: Calculated ground-state properties of silicon carbide. J. Phys. C **19**, 4413 (1986)

62. Weber, W.J., Yu, N., Wang, L.M., Hess, N.J.: Temperature and dose dependence of ion-beam-induced amorphization in α-SiC. J. Nucl. Mater. **244**, 258 (1997)

63. Tang, M., Yip, S.: Lattice instability in β-SiC and simulation of brittle fracture. J. Appl. Phys. **76**, 2719 (1994)

64. Weber, W.J., Yu, N., Wang, L.M., Hess, N.: Structure and properties of ion-beam-modified (6H) silicon carbide. J. Mater. Sci. Eng. A **253**, 62 (1998)

65. Gao, F., Weber, W.J.: Mechanical properties and elastic constants due to damage accumulation and amorphization in SiC. Phys. Rev. B **69**, 224108 (2004)

66. Vukcevich, M.R.: The elastic constants of cubic crystals with covalent and partially covalent bonds. Phys. Stat. Solidi (b) **54**, 435 (1972)

67. Barsch, G.R.: Relation between third-order elastic constants of single crystals and polycrystals. J. Appl. Phys. **39**, 3780 (1968)

68. Hill, R.: The elastic behavior of a crystalline aggregate. Proc. Phys. Soc. (Lond.) **65A**, 349 (1952)

69. Voigt, W.: Lehrbuch der Kristallphysik. Teubner, Leipzig (1928)

70. Reuss, A.: Calculation of the flow limits of mixed crystals on the basis of the plasticity of monocrystals. Angew Z. Math. Mech. **9**, 49 (1929)

71. Takahiro, M., Tetsuro, N., Yasuaki, N., Katsuhiro, K., Tastuya, Y., Hidetoshi, N., Satoshi, N.: Measurement of high-temperature elastic properties of ceramics using a laser ultrasonic method. J. Am. Ceram. Soc. **84**, 1521–1525 (2001)

72. Pugh, S.F.: Relations between the elastic moduli and the plastic properties of polycrystalline pure metals. Philos. Mag. **45**, 823 (1954)

73. Frantsevich, N., Voronov, F.F., Bokuta, S.A.: In: Frantsevich, I. N. (ed.) Elastic Constants and Elastic Moduli of Metals and Insulators Handbook, vol. 60. Naukova Dumka, Kiev (1983)

74. Schreiber, E., Anderson, O.L., Soga, N.: Elastic constants and Their Measurements. McGraw-Hill, New York (1973)

75. Harrison, W.A.: Electronic Structure and Properties of Solids. Dover, New York (1989)

76. Bouhemadou, A., Khenata, R., Kharoubi, M., Seddik, T., Reshak, A.H., Al-Douri, Y.: FP-APW+ lo calculations of the elastic properties in zinc-blende III-P compounds under pressure effects. Comput. Mater. Sci **45**, 474 (2009)

77. Maachou, A., Aboura, H., Amrani, B., Khenata, R., Bin Omran, S., Varshney, D.: Structural stabilities, elastic and thermodynamic properties of scandium chalcogenides via first-principles calculations. Comput. Mater. Sci. **50**, 3123 (2011)

78. Kleinman, L.: Deformation potentials in silicon. I. Uniaxial strain. Phys. Rev. **128**, 2614 (1962)

79. Kim, K., Lambrecht, W.R.L., Segal, B.: Electronic structure of GaN with strain and phonon distortions. Phys. Rev. B **50**, 1502 (1994)

80. Blackman, M. The specific heat of solids. Proc. R. Soc. Lond. A 1942; **181**:58; *ibid* 1937; **159**: 416; 1935; **149**:126; 1935; **148**:384; 1935; **148**:365

81. Blackman, M.: The specific heat of solids. Proc. R. Soc. Lond. A **159**, 416 (1937)

82. Blackman, M.: The specific heat of solids. Proc. R. Soc. Lond. A **149**, 126 (1935)

83. Blackman, M.: The specific heat of solids. Proc. R. Soc. Lond. A **148**, 384 (1935)

84. Blackman, M.: The specific heat of solids. Proc. R. Soc. Lond. A **148**, 365 (1935)

85. Gopal, E.S.R.: Specific heats at low temperatures. Plenum Press, New York (1966)

86. Tari, A.: The Specific Heat of Matter at Low Temperatures. Imperial College Press, London (2003)